Published by Institute of Physics Publishing for SISSA
Received: *August 5, 2007*
Accepted: *October 29, 2007*
Published: *November 14, 2007*

MSSM effects in top-antitop production at the LHC

D.A. Ross

School of Physics & Astronomy, University of Southampton, Southampton SO17 1BJ, United Kingdom
E-mail: dar@phys.soton.ac.uk

M. Wiebusch

Institut für Theoretische Physik, RWTH Aachen, 52056 Aachen, Germany
E-mail: martin.wiebusch@physik.rwth-aachen.de

Abstract: We report on a calculation of the effects of supersymmetry on the cross-section for top-antitop production at LHC. A numerical study is carried out for the ten benchmarks of the Snowmass accord. It is found that the higher order effects involving supersymmetric particles in internal loops can be as high as 6%, both for the cross-section and the (parity even) helicity asymmetry, for one particular benchmark. For other benchmarks smaller but nonetheless observable corrections are found.

Keywords: Supersymmetry Phenomenology, Supersymmetric Standard Model.

JHEP11(2007)041

Contents

1. Introduction

For nearly 35 years, supersymmetry (SUSY) has been an attractive theory in particle physics [1, 2]. At the most theoretical level, it permits the construction of string theories which do not contain tachyonic states, and at the phenomenological level it offers a solution to the hierarchy problem through its reduced ultraviolet divergences, as well as providing resolutions of several puzzles arising in standard models of cosmology. It also gives rise to a correction to the running of the couplings, so that the strong, weak, and electromagnetic interactions can unify at some Grand Unified (GUT) scale.

However, to date there has been no reliable evidence that this theory describes Nature, so that if SUSY is indeed realised in nature, it must be broken at a scale higher than that reached in accelerator experiments conducted up to now. If the theory is to be effective in providing a solution to the hierarchy problem, then the SUSY breaking scale cannot be much more than about 1 TeV. This is also the scale of SUSY breaking which leads to unification of couplings. Hence, with the exception of some hidden corners of parameter space, SUSY can be discovered at the forthcoming LHC.

Clearly the most dramatic manifestation of SUSY would be the production and identification of supersymmetric partner particles such as the spin-$\frac{1}{2}$ charginos or neutralinos, or evidence that at sufficiently high energies hadrons display behaviour consistent with the existence of squarks or gluinos. However, the existence of SUSY will also have indirect but measurable effects on the (total and differential) cross-sections for the production of Standard Model (SM) particles. The LHC is expected to achieve sufficient integrated luminosity so that the statistical errors on these cross-sections are below the percent level. Assuming

sufficient control over theoretical and experimental systematic errors, we will then be able to detect the effects of higher order corrections coming from loops of SUSY particles. The loops can give rise to a significant correction to the production cross-sections even below the threshold for the production of the SUSY particles themselves, so that hints that some new physics is imminent can be deduced before the threshold energies are actually reached. Above these thresholds, differential cross-sections with respect to suitably chosen variables can display structures which can be used to experimentally constrain the parameters of the underlying model.

Due to its large mass the top quark decays predominantly via electroweak interactions. Since the electroweak interactions violate parity, information about the spin of the top quark is encoded in the angular distribution of its decay products [3]. To fully exploit future experimental data we therefore need accurate computations (within the SM and beyond) of *polarised* $t\bar{t}$ production amplitudes, i.e. amplitudes for the production of $t\bar{t}$ pairs with given helicities. Such amplitudes allow us to predict not only the total $t\bar{t}$ cross section but also single and double spin asymmetries like the ones discussed in [4]. Of particular interest are parity violating asymmetries, since they are free of QCD related systematic errors. Considering ratios of asymmetries and total cross sections also removes systematic errors related to uncertainties in the incident beam flux.

The SM predictions for hadronic $t\bar{t}$ production have already been calculated by several groups. Tree level amplitudes were first considered in [5 – 10]. The next-to-leading order (NLO) QCD corrections to unpolarised amplitudes have been calculated in [11 – 16] and the electroweak contributions ($\mathcal{O}(\alpha\alpha_s^2)$) have been studied in [17 – 20]. Soft gluon resummation and threshold effects have been considered in [21 – 25]. The NLO QCD and electroweak corrections to polarised amplitudes are presented in [26 – 29] and [20, 30 – 34], respectively. The estimates for the theoretical errors of these calculations lie at the percent level.

Partial studies of SUSY contributions to both unpolarised and polarised $t\bar{t}$ production amplitudes within the Minimal Supersymmetric SM (MSSM) also exist. The SUSY electroweak corrections to unpolarised amplitudes are calculated in [35 – 37]. The same study for polarised amplitudes is carried out in [30]. The NLO SUSY QCD (SQCD) corrections to top production via gluon fusion ($gg \to t\bar{t}$) are presented in [38, 39]. Top production via quark-antiquark annihilation is discussed in [40 – 42]. During the preparation of this paper a complete study of NLO SQCD corrections [43] was also published. As pointed out there, the results of [40 – 42] disagree due to an incorrect treatment of Majorana fermions in box diagrams. For the SQCD corrections we see the same qualitative features as those reported in [43], especially the structure of the differential cross-section with respect to the invariant mass of the $t\bar{t}$ pair. However, a precise numerical comparison of our results is not straightforward due to a different choice of renormalisation schemes and is therefore not carried out in this paper.

In this paper we present a complete study of SUSY QCD and electroweak corrections to $t\bar{t}$ production within the MSSM framework. We have organised our calculation so that software is available to calculate differential cross-sections with all possible helicity configurations and any given set of the extra 105 parameters of the MSSM. This provides maximum flexibility for studying different SUSY breaking scenarios and exotic areas of

JHEP11(2007)041

the parameter space, even though a scan over all 105 parameters is clearly unrealistic. Our code can read input parameters in the SUSY Les Houches Accord format [44], which makes it easily combinable with other MSSM related software. As a first analysis we present numerical results for the 10 'Snowmass' benchmark points of the MSSM parameter space, which were compiled at the Snowmass meeting of 2002 [45]. We find considerable variation in the magnitudes of the corrections from these different parameter sets. Conversely, this means that accurate measurement of the $t\bar{t}$ production cross-section can be used as a tool to help identify the correct set of SUSY parameters.

At sufficiently high (partonic) energies, the SUSY corrections to $t\bar{t}$ production are expected to be dominated by single and double logarithms of incoming parton energy divided by the SUSY breaking scale, M_{SUSY}. The determination of these logarithms is independent of the SUSY parameter set, with the exception of M_{SUSY} and the ratio, $\tan\beta$, of the vacuum expectation values of the two Higgs doublets, and the calculation is simplified by the fact that the mixing of various SUSY particles to form mass eigenstates has no effect on these logarithms. The logarithmic contributions have been calculated by Beccaria et. al. [46]. One may have expected that it would have been possible to express the entire SUSY correction in terms of these logarithms plus a constant off-set, which depended on the SUSY parameter set. We have compared our results with those of [46] and although it is indeed the case that our results agree with these logarithms plus a constant off-set at sufficiently high partonic energies, this approximation is found to be unsuitable at typical partonic energies which will be reached at the LHC, and the entire calculation is required for a reliable prediction of the cross-sections at the LHC.

The structure of this paper is as follows: In section 2 we discuss the general method for the extraction of the above-mentioned helicity matrix-elements at the partonic level from a general Feynman graph. In section 3 we list all the prototype graphs and indicate which supersymmetric particles can contribute for each of the prototypes. In section 4 we discuss the results after folding the partonic cross-sections with PDFs and show the results for the ten Snowmass benchmark points. Section 5 presents some conclusions.

2. Helicity matrix elements

Because we wish to discuss the total and differential cross-sections for given helicities of the t- and $\bar{t}$- quarks as well as the asymmetries, we find it convenient to work at the parton level with generic processes

$$\begin{aligned} g(p_a,\lambda_a)\, g(p_b,\lambda_b) &\to t(p_1,\lambda_1)\, \bar{t}(p_2,\lambda_2) \quad , \\ q(p_a,\lambda_a)\, \bar{q}(p_b,\lambda_b) &\to t(p_1,\lambda_1)\, \bar{t}(p_2,\lambda_2) \quad , \end{aligned}$$

where g, t ($\bar{t}$) and q ($\bar{q}$) denote gluons, top and massless (anti-)quarks, respectively, p_a, p_b, p_1 and p_2 are the corresponding four-momenta and λ_a, λ_b, λ_1 and λ_2 the helicities. The amplitudes $\mathcal{A}^{gg/q\bar{q}}_{\lambda_a,\lambda_b,\lambda_1,\lambda_2}(E,\theta)$ for the processes above we call helicity matrix-elements and consider them as functions of the partonic centre-of-mass energy E and scattering angle θ (also in the centre-of-mass frame).

In the case of quark-antiquark annihilation, for which we take the incoming quarks and antiquarks to be massless, the helicities of the incoming partons are anti-correlated ($\lambda_a = -\lambda_b$) at leading order. Although it is possible for this initial anti-correlation to be violated at the one-loop level, the interferences at $\mathcal{O}(\alpha_s^3)$ or $\mathcal{O}(\alpha_s^2\alpha_W)$ always respect this anti-correlation. For the gluon fusion process there is no such correlation.

Once these helicity matrices have been determined, differential cross-sections and asymmetries can be computed by convolution with the corresponding parton distribution functions (PDF), summed over helicities or not, as appropriate.

A further potential advantage of computing helicity matrix-elements, although not currently applicable at LHC, is the determination of initial beam polarisation asymmetries, should it become possible in the future to polarise these beams. For interactions of a parity violating nature such as SUSY corrections to weak interactions, such asymmetries would be immensely useful in identifying the parameters of the supersymmtery model.

The helicity amplitudes are obtained in two stages. In the first stage, a set of coefficient functions, $a^{\{\alpha\}}_{\lambda_a,\lambda_b}(E,\theta)$, of a complete set of spinor matrices is determined:

$$\mathcal{A}_{\lambda_a,\lambda_b,\lambda_1,\lambda_2}(E,\theta) \;=\; \sum_{\{\alpha\}} a^{\{\alpha\}}_{\lambda_a,\lambda_b}(E,\theta)\bar{u}(p_1,\lambda_1)\Gamma^{\{\alpha\}}v(p_2,-\lambda_2) \tag{2.1}$$

where $\Gamma^{\{\alpha\}}$ are the matrices

$$\begin{aligned}\Gamma^{\mu}_{V} &= \gamma^{\mu}\\ \Gamma^{\mu}_{A} &= \gamma^{\mu}\gamma^{5}\\ \Gamma^{\mu\nu}_{T} &= \sigma^{\mu\nu}\end{aligned} \tag{2.2}$$

with associated projection operators $P^{\{\alpha\}}$

$$\begin{aligned}P^{\mu}_{V} &= \frac{1}{4}\left(\gamma^{\mu} + \frac{p_1^{\mu}}{m_t}\right)\\ P^{\mu}_{A} &= \frac{1}{4}\left(\gamma^{5}\gamma^{\mu} + \gamma^{5}\frac{p_1^{\mu}}{m_t}\right)\\ P^{\mu\nu}_{T} &= \frac{1}{8}\sigma^{\mu\nu},\end{aligned} \tag{2.3}$$

such that

$$\mathrm{Tr}\left(\Gamma^{\{\alpha\}}P_{\{\beta\}}\right) \;=\; \delta^{\{\alpha\}}_{\{\beta\}}.$$

Note that the coefficient functions are independent of the helicities of the t- and $\bar{t}$ quarks

For the basis vectors $e_0 \cdots e_3$, where

$$\begin{aligned}e_0^{\mu} &= \frac{1}{2E}\left(p_1^{\mu} + p_2^{\mu}\right)\\ e_1^{\mu} &= \frac{1}{2Ep\sin\theta}\left(-(p + E\cos\theta)p_1^{\mu} + (p - E\cos\theta)p_2^{\mu} + 2p\,p_a^{\mu}\right)\\ e_2^{\mu} &= \frac{1}{2E^2p\sin\theta}\varepsilon^{\mu}_{\nu\rho\sigma}p_1^{\nu}p_2^{\rho}p_a^{\sigma}\\ e_3^{\mu} &= \frac{1}{2p}\left(p_1^{\mu} - p_2^{\mu}\right)\end{aligned}$$

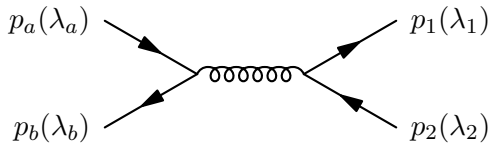

Figure 1: Tree-level graph for $t-\bar{t}$ production from quark-antiquark annihilation.

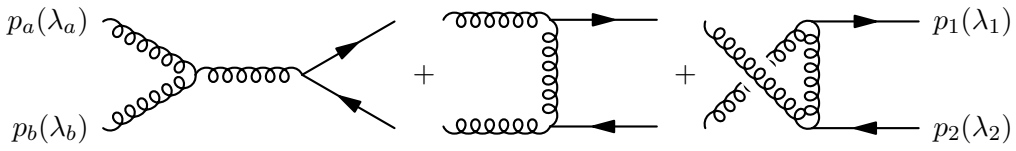

Figure 2: Tree-level graphs for $t-\bar{t}$ production from gluon fusion.

(p being the magnitude of the three-momentum of the t-quark in the centre-of-mass frame), the helicity matrix elements are given by[1]

$$\begin{aligned}\mathcal{A} = & 2\left[E\left(-a_V^1 + i\lambda_1 a_V^2\right) + ip\left(a_A^2 + i\lambda_1 a_A^1\right) - im_t\left(a_T^{01} - i\lambda_1 a_T^{02}\right)\right]\delta_{\lambda_1,-\lambda_2} \\ & + 2\left[m_t\, a_A^0 - p\, a_T^{12} - i\, E\,\lambda_1 a_T^{03} - m_t\,\lambda_1 a_V^3\right]\delta_{\lambda_1,\lambda_2} \end{aligned} \tag{2.4}$$

Thus, for example, the non-zero coefficient functions for the quark-antiquark annihilation process at the tree-level (figure 1) are:

$$\begin{aligned} a_V^1 &= g_s^2 \frac{\cos\theta}{2E}\delta_{\lambda_a,-\lambda_b}\left(\boldsymbol{\tau}\otimes\boldsymbol{\tau}\right) \\ a_V^2 &= g_s^2 \frac{i\lambda_a}{2E}\delta_{\lambda_a,-\lambda_b}\left(\boldsymbol{\tau}\otimes\boldsymbol{\tau}\right) \\ a_V^1 &= g_s^2 \frac{\sin\theta}{2E}\delta_{\lambda_a,-\lambda_b}\left(\boldsymbol{\tau}\otimes\boldsymbol{\tau}\right), \end{aligned} \tag{2.5}$$

where $(\boldsymbol{\tau}\otimes\boldsymbol{\tau})$ indicates the colour factor for a single gluon exchange. Inserting these expressions for the coefficents into eq. (2.4) generates the helicity matrix-element

$$\begin{aligned}\mathcal{A}_{\lambda_a,\lambda_b,\lambda_1,\lambda_2}(E,\theta) = & -g_s^2\left(\lambda_a + \cos\theta\right)\delta_{\lambda_a,-\lambda_b}\delta_{\lambda_1,-\lambda_2}\left(\boldsymbol{\tau}\otimes\boldsymbol{\tau}\right) \\ & -g_s^2\frac{m_t}{E}\lambda_1\sin\theta\,\delta_{\lambda_a,-\lambda_b}\delta_{\lambda_1,\lambda_2}\left(\boldsymbol{\tau}\otimes\boldsymbol{\tau}\right), \end{aligned} \tag{2.6}$$

whereas for the gluon fusion process (figure 2), the non-zero coefficients are given by

$$\begin{aligned} a_V^1 = & \frac{g_s^2}{2E(E-p\cos\theta)}\tau^b\tau^a\left\{E\sin\theta\left(\cos\theta-2\right)\delta_{\lambda_a,\lambda_b} + 2p\sin\theta\cos\theta\right\} \\ & + \Big[\tau^a\leftrightarrow\tau^b,\ \lambda_a\leftrightarrow\lambda_b,\ \theta\to(\pi+\theta)\Big] \\ a_V^2 = & \frac{ig_s^2}{2E(E-p\cos\theta)}\tau^b\tau^a p\,\sin\theta\,\lambda_a\delta_{\lambda_a,-\lambda_b} \quad + \Big[\tau^a\leftrightarrow\tau^b,\ \lambda_a\leftrightarrow\lambda_b,\ \theta\to(\pi+\theta)\Big] \end{aligned}$$

[1]These matrix-elements are defined up to an overall phase, which may depend on the initial-state and final-state helicities.

$$
\begin{aligned}
a_V^3 &= \frac{g_s^2}{2E(E-p\cos\theta)}\tau^b\tau^a\left\{-E\cos\theta\left(\cos\theta-2\right)\delta_{\lambda_a,\lambda_b}+2p\sin^2\theta\right\}\\
&\quad+\Big[\tau^a\leftrightarrow\tau^b,\ \lambda_a\leftrightarrow\lambda_b,\ \theta\to(\pi+\theta)\Big]\\
a_A^0 &= \frac{g_s^2}{2E(E-p\cos\theta)}\tau^b\tau^a\lambda_a\left(p\cos\theta-E\right)\delta_{\lambda_a,\lambda_b}\\
&\quad+\Big[\tau^a\leftrightarrow\tau^b,\ \lambda_a\leftrightarrow\lambda_b,\ \theta\to(\pi+\theta)\Big]\\
a_T^{12} &= \frac{g_s^2}{2E(E-p\cos\theta)}\tau^b\tau^a m_t\cos\theta\delta_{\lambda_a,\lambda_b}\quad+\Big[\tau^a\leftrightarrow\tau^b,\ \lambda_a\leftrightarrow\lambda_b,\ \theta\to(\pi+\theta)\Big]
\end{aligned}
\tag{2.7}
$$

leading to a tree-level helicity matrix-element

$$
\begin{aligned}
\mathcal{A}_{\lambda_a,\lambda_b,\lambda_1,\lambda_2}(E,\theta) &= \frac{g_s^2}{2E(E-p\cos\theta)}\tau^b\tau^a\\
&\quad\times\Bigg\{m_t\left[2\lambda_1\left((E+p)\cos^2\theta-2p-4E\cos\theta\right)-2\lambda_a E\right]\delta_{\lambda_1,\lambda_2}\delta_{\lambda_a,\lambda_b}\\
&\quad\left[-2E(E+p)\cos\theta\sin\theta+4E^2\sin\theta\right]\delta_{\lambda_1,-\lambda_2}\delta_{\lambda_a,\lambda_b}\\
&\quad-2\lambda_1 p\,m_t\sin^2\theta\delta_{\lambda_1,\lambda_2}\delta_{\lambda_a,-\lambda_b}\\
&\quad-Ep\sin\theta\left(2\cos\theta+\lambda_1\lambda_a\right)\delta_{\lambda_1,-\lambda_2}\delta_{\lambda_a,-\lambda_b}\Bigg\}\\
&\quad+\Big[\tau^a\leftrightarrow\tau^b,\ \lambda_a\leftrightarrow\lambda_b,\ \theta\to(\pi+\theta)\Big]
\end{aligned}
\tag{2.8}
$$

In the case of gluon fusion the contribution from any graph may be written in the form

$$\bar{u}(p_1,\lambda_1)\Gamma v(p_2,-\lambda_2),$$

where Γ is a sum of strings of γ-matrices with coefficients that are proportional to couplings, internal and external fermion masses and the Veltman-Passarino (VP) [47] functions arising from the loop integrals. These VP functions have arguments that depend on the internal and external masses as well as on the Mandelstam variables s,t,u. The coefficients $a^{\{\alpha\}}$ are simply projected by

$$a^{\{\alpha\}} \;=\; \mathrm{Tr}\left(P^{\{\alpha\}}\Gamma\right). \tag{2.9}$$

For the quark-antiquark annihilation process there are two types of contributing graphs: The first type are graphs for which the fermion lines can be factorised into an initial quark line, Γ^i and a final t-quark line, Γ_f. Again these are sums of string of γ-matrices with coefficients that are proportional to VP functions. In this case the coefficients $a^{\{\alpha\}}$ are projected by

$$a^{\{\alpha\}} \;=\; \delta_{\lambda_a,-\lambda_b}\mathrm{Tr}\left(\Gamma_i\gamma\cdot v\frac{\left(1-\lambda_a\gamma^5\right)}{2}\right)\mathrm{Tr}\left(P^{\{\alpha\}}\Gamma_f\right), \tag{2.10}$$

where v^μ is a vector in the plane normal to the incoming momenta p_a and p_b given by:

$$v^\mu \;=\; \frac{1}{\sqrt{2}E\,p\,\sin\theta}\left\{p_b\cdot p_1 p_a^\mu+p_a\cdot p_1 p_b^\mu-p_a\cdot p_b p_1^\mu+i\lambda_a\varepsilon^\mu_{\nu\rho\sigma}p_a^\nu p_b^\rho p_1^\sigma\right\}$$

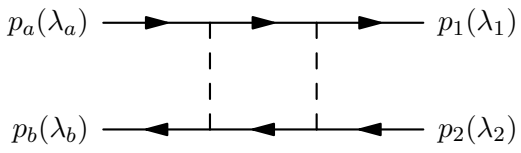

Figure 3: Gluino, neutralino, or chargino exchange contribution to $t - \bar{t}$ production from quark-antiquark annihilation

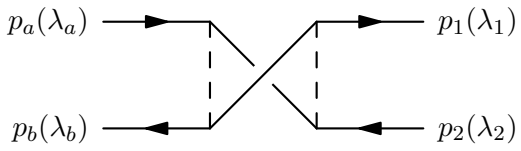

Figure 4: Graph involving the exchange of intermediate Majorana fermions

The other type of graph is one in which the fermion lines do *not* factorise into an initial fermion line and a final-fermion line, but rather into an upper line, Γ_u, and a lower line, Γ_d, in which the incoming quark and outgoing t-quarks are connected by the exchange gluino, neutralinos, and charginos,is the s-channel. It is graphs of this type that give rise to non-zero amplitudes in the case where the incoming helicities are equal, but such amplitudes do not interfere with the tree-level amplitudes. An example of such a graph is shown in figure 3. For such graphs the coefficients $a^{\{\alpha\}}$ are projected by

$$a^{\{\alpha\}} = \mathrm{Tr}\left(\Gamma_d \gamma \cdot v \frac{\left(1 - \lambda_a \gamma^5\right)}{2}\right) \Gamma_d P^{\{\alpha\}} \tag{2.11}$$

As in the case of most of the contributing graphs, the expressions obtained from figure 3 for the corrections to the coefficients are too long and unwieldy to be reproduced here.

Finally we note here that in several cases, the internal fermions exchanged in the s-channel in such graphs may be neutralinos or gluinos, which are Majorana fermions. In such cases supplementary graphs of the type shown in figure 4 need to be considered. Great care needs to be taken in handling such graphs. The standard expressions for the propagators of Majorana fermions in which a fermion propagates into a fermion or an anti-fermion propagates into an anti-fermion, are ambiguous up to a sign until the exact ordering of the fermions is determined. In order to ensure that this is effected in a consistent manner it is necessary to determine the fermion ordering of the term in the Wick contraction corresponding to the graph under consideration.

A library has been constructed both in FORTRAN and C++ in which each of the prototype graphs shown in the next section can be determined numerically, as a function of the incoming energy, scattering angle, helicities, couplings and internal masses. We have checked all prototype graphs by selecting different routings of the internal loop momenta and copmparing the results numerically. The numerical values of of the relevant VP functions are determined either using the `FF` library [48] or `LoopTools` [49] These libraries can be found at `http://hep.phys.soton.ac.uk/hepwww/staff/D.Ross/susyttbar/`

3. Diagrams

In this section we list the diagrams needed for the computation of SUSY contributions to polarised top-antitop production cross sections. To save space we only draw the different *topologies*. For further reference, each topology has a label set in typewriter font. An asterisk behind the label indicates that the crossed version of this diagram has to be included as well. A double asterisk indicates that *only* the crossed version is needed. First or second generation quarks are labelled q and top quarks are labelled t. Gluons are denoted as g and always represented by curly lines. Momenta and helicities are given in parentheses behind the label. For example, $t(p, \lambda)$ denotes a top quark with (four-)momentum p and helicity λ. The generic scalar, vector and fermionic particles in each topology are given uppercase labels S, V, F, etc. For each topology we provide a list of MSSM particles that have to be substituted for the generic ones. For the various MSSM particles we use the notations from [50]. However, unless stated otherwise the generation indices I, J, etc. only run over the first two generations. The third generation quarks are written explicitly as t $(= u^3)$ and b $(= d^3)$.

3.1 Tree-level diagrams

The following prototype diagrams contribute to $t\bar{t}$ production at tree-level:

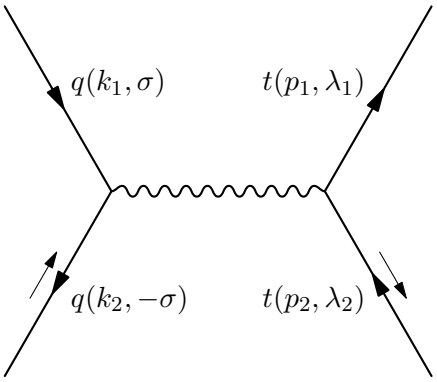

`Dqqbar_sV_tree`
$V = \gamma, Z, g$

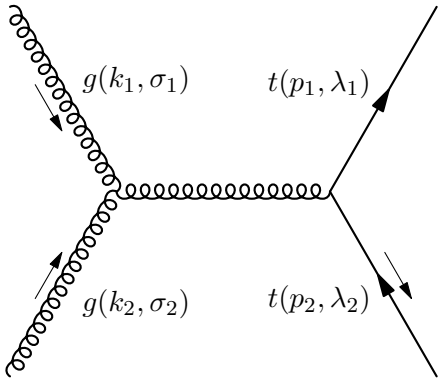

`Dgg_sG_tree`

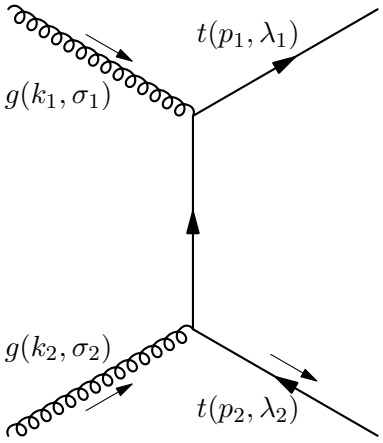

`Dgg_tF_tree`*
$F = t$

3.2 Self-energy diagrams

For our calculation we only need to consider self-energy corrections for fermions and gluons. The SUSY self-energy corrections to fermion propagators only come from scalar particles:

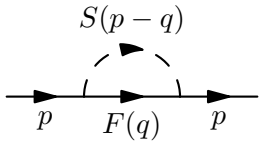

(3.1)

The s-channel gluon propagator gets SUSY corrections from fermion and scalar loops:

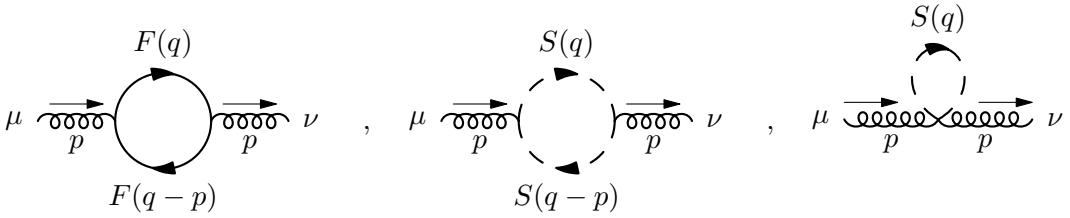

(3.2)

The two scalar self-energy diagrams always appear as a pair with the same coefficient and the same scalar particle in the loop. By inserting these self-energy corrections in individual lines of the tree level diagrams we obtain the following *self-energy diagrams*:

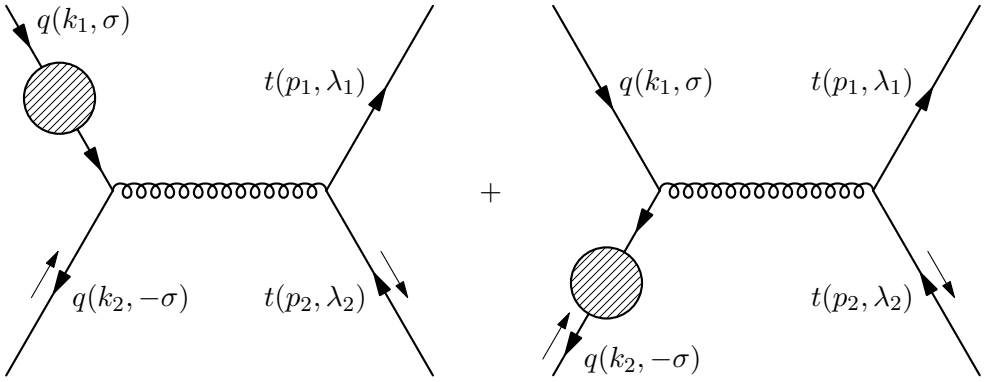

`Dqqbar_sV_xseSq`

$(q,F,S) = (u^I,\chi_j^0,U_i),\ (d^I,\chi_j^0,D_i),\ (u^I,\chi_j,D_i),\ (d^I,\chi_j^c,U_i),\ (u^I,\Lambda,U_i),\ (d^I,\Lambda,D_i)$

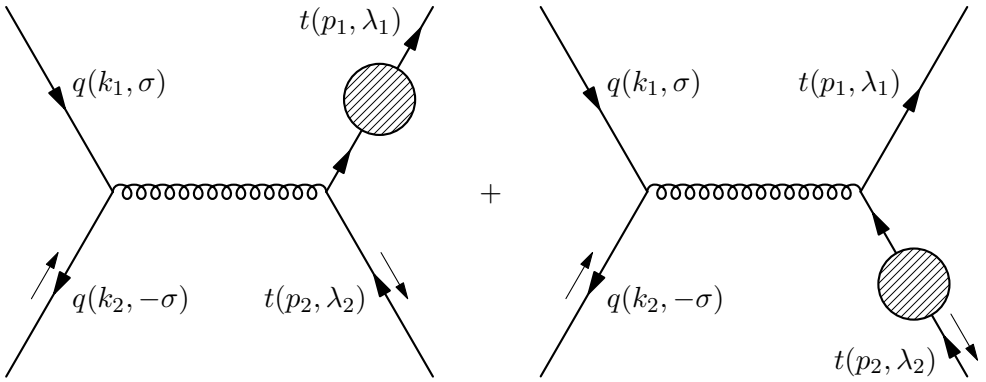

`Dqqbar_sV_xseSt`

$(F,S) = (\chi_j^0,U_i),\ (\chi_j,D_i),\ (t,H_i^0),\ (t,A_1^0),\ (b,H_1),\ (\Lambda,U_i)$

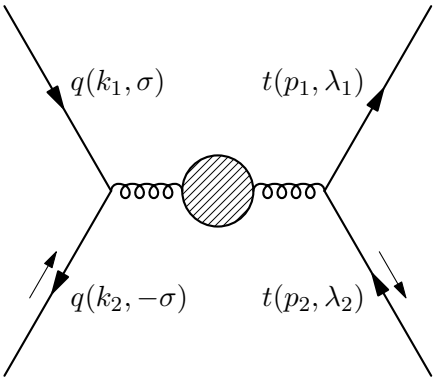

`Dqqbar_sG_iseF`, `Dqqbar_sG_iseS`

$q = u^I, d^I \quad , \quad F = u^I, t, d^I, b, \Lambda \quad , \quad S = U_i, D_i$

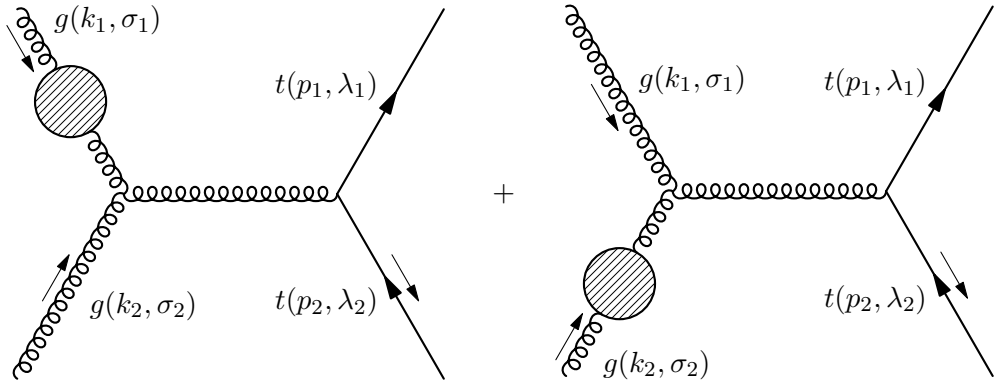

`Dgg_sG_xseFg`, `Dgg_sG_xseSg`

$F = \Lambda \quad , \quad S = U_i, D_i$

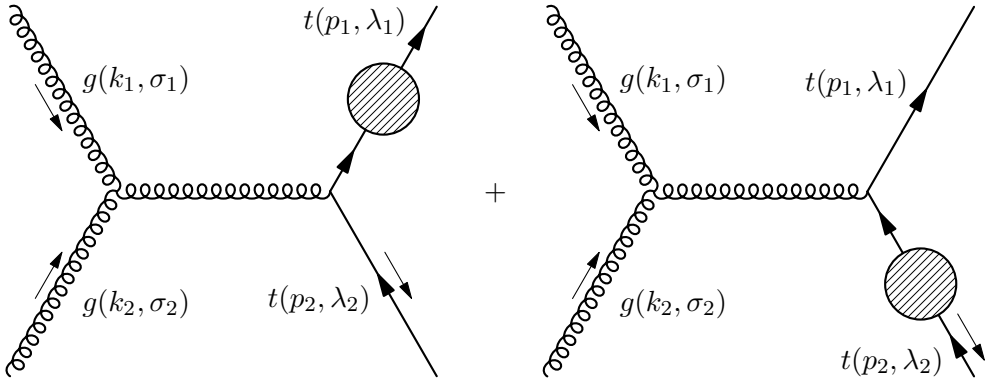

`Dgg_sG_xseSt`

$(F, S) = (\chi_j^0, U_i),\ (\chi_j, D_i),\ (t, H_i^0),\ (t, A_1^0),\ (b, H_1),\ (\Lambda, U_i)$

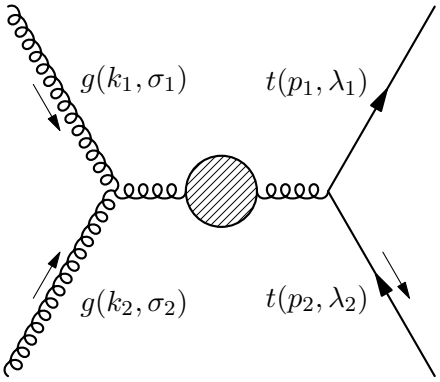

`Dgg_sG_iseF`, `gg_sG_iseS`

$F = \Lambda \quad , \quad S = U_i, D_i$

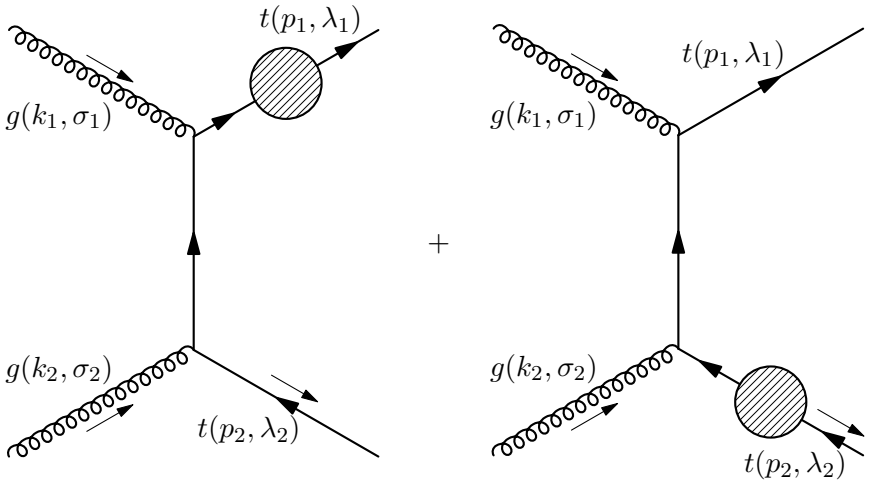

`Dgg_tF_xseSt`*

$(F,S) = (\chi_j^0, U_i),\ (\chi_j, D_i),\ (t, H_i^0),\ (t, A_1^0),\ (b, H_1),\ (\Lambda, U_i)$

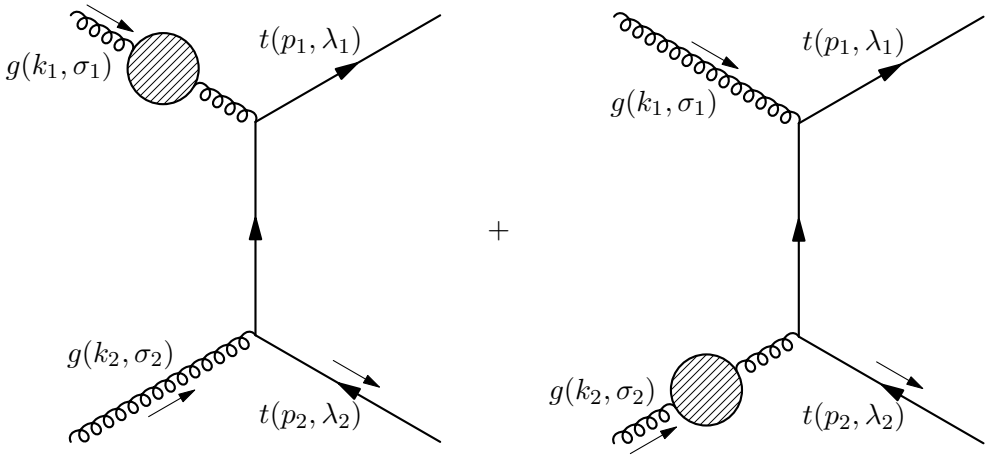

`Dgg_tF_xseSt`*

$F = \Lambda \quad , \quad S = U_i, D_i$

JHEP11(2007)041

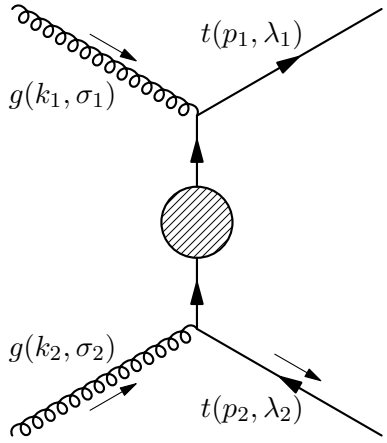

`Dgg_tF_iseS`*

$(F, S) = (\chi_j^0, U_i),\ (\chi_j, D_i),\ (t, H_i^0),\ (t, A_1^0),\ (b, H_1),\ (\Lambda, U_i)$

In each diagram the hatched blob stands for one of the self-energy corrections from (3.1) or (3.2).

3.3 Vertex corrections

The prototype vertex corrections for the $q\bar{q} \to t\bar{t}$ amplitude are:

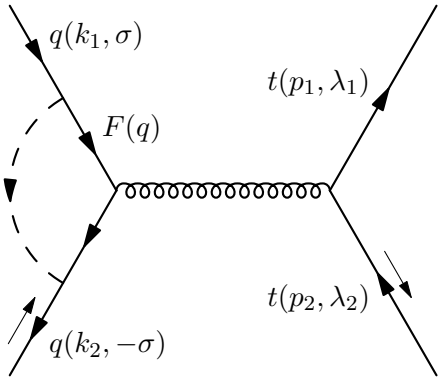

`Dqqbar_sG_vertSq`

$(q, F, S) = (u^I, \Lambda, U_i),\ (d^I, \Lambda, D_i)$

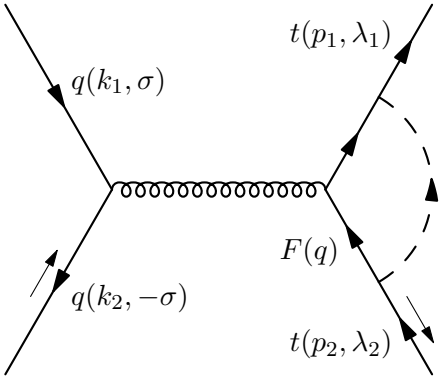

`Dqqbar_sV_vertSt`

$q = u^I, d^I$

$(F, S) = (\Lambda, U_i),\ (t, H_1^0),\ (t, A_1^0),\ (b, H_1)$

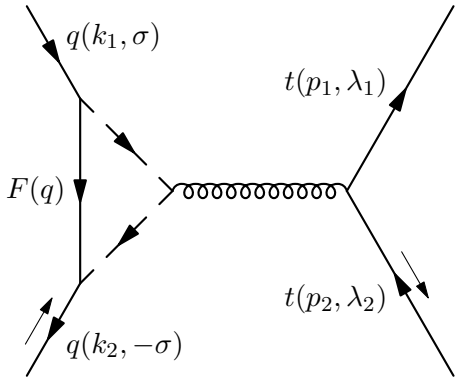

`Dqqbar_sG_vertSSq`

$(q,F,S) =$
$(u^I,\Lambda,U_i),\ (u^I,\chi_j^0,U_i),\ (u^I,\chi_j,D_i),$
$(d^I,\Lambda,D_i),\ (d^I,\chi_j^0,D_i),\ (d^I,\chi_j,U_i)$

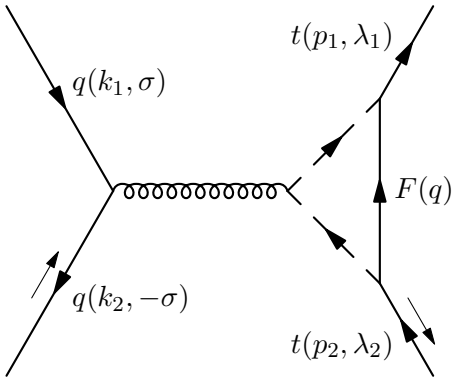

`Dqqbar_sG_vertSSt`

$q = u^I, d^I$
$(S,F) = (\Lambda,U_i),\ (\chi_j^0,U_i),\ (\chi_j,D_i)$

For the $gg \to t\bar{t}$ amplitude we distinguish vertex corrections for s and t-channel diagrams. The corrections to the s-channel diagrams are:

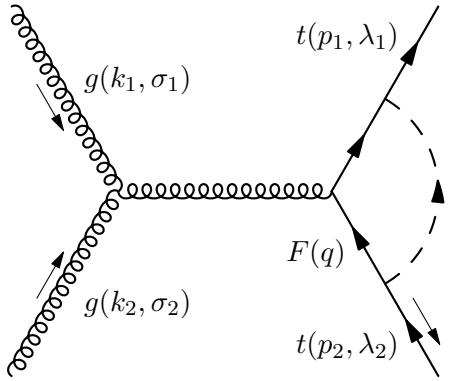

`Dgg_sG_vertSt`

$(F,S) = (\Lambda,U_i),\ (t,H_1^0),\ (t,A_1^0),\ (b,H_1)$

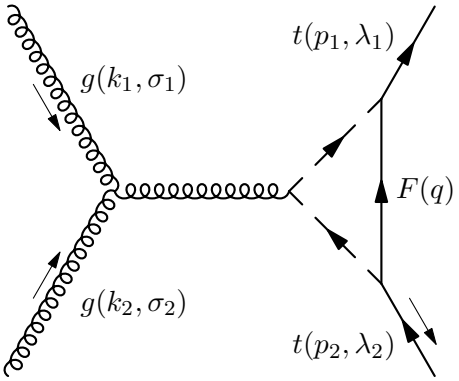

`Dgg_sG_vertSSt`

$(S,F) = (U_i,\Lambda),\ (U_i,\chi_j^0),\ (D_i,\chi_j)$

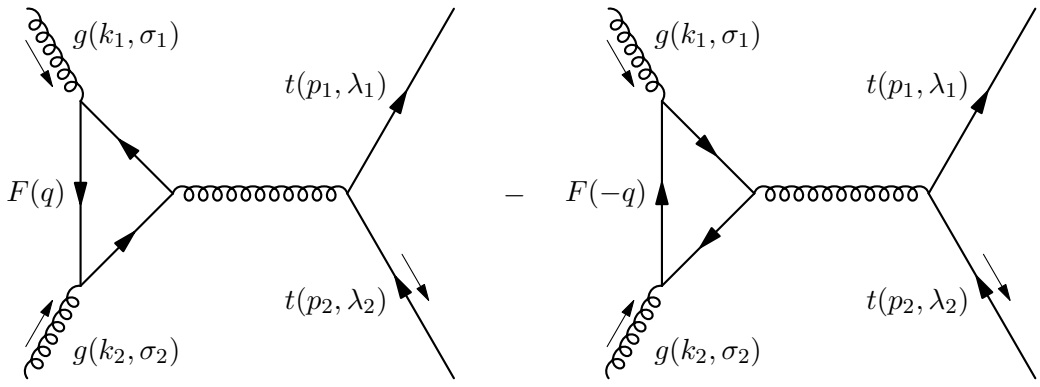

`Dgg_sG_vertFg`

$F = \Lambda$

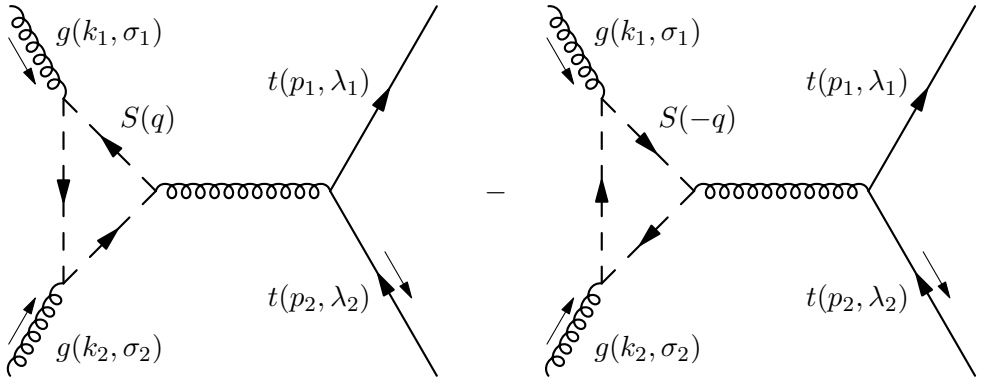

`Dgg_sG_vertSg`

$S = U_i, D_i$

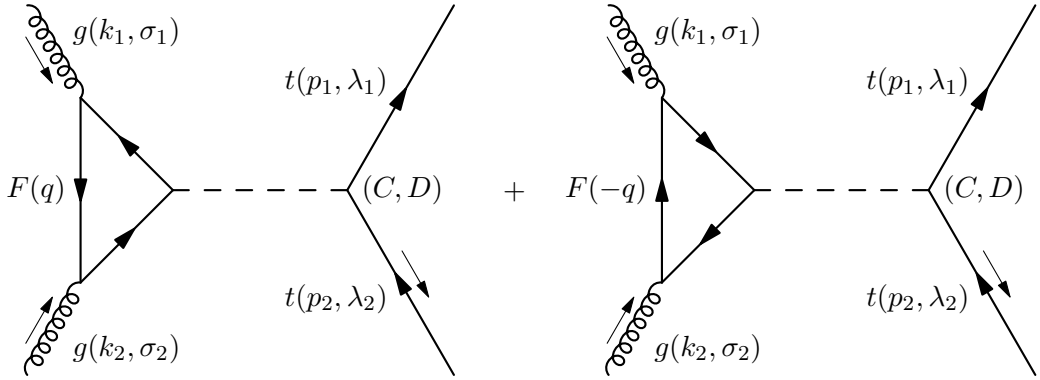

`Dgg_sS_vertFg`

$F = t, b \quad , \quad S = H_1^0, A_1^0$

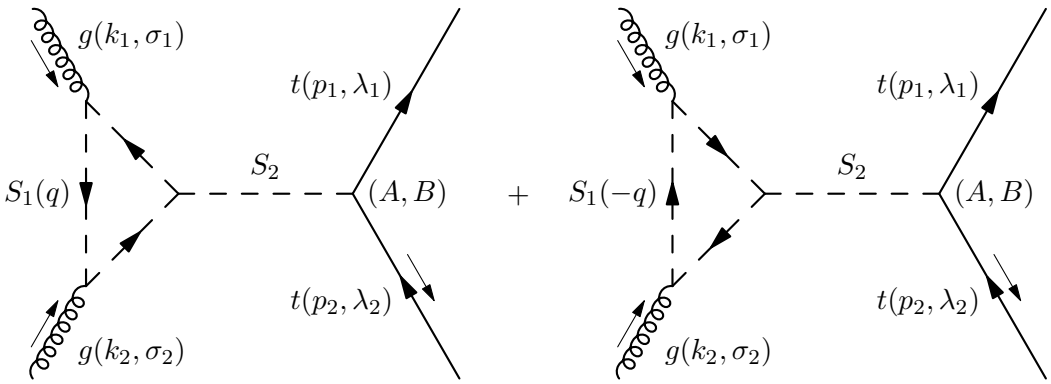

`Dgg_sS_vertSg`

$S_1 = U_i, D_i \quad , \quad S_2 = H_1^0, A_1^0$

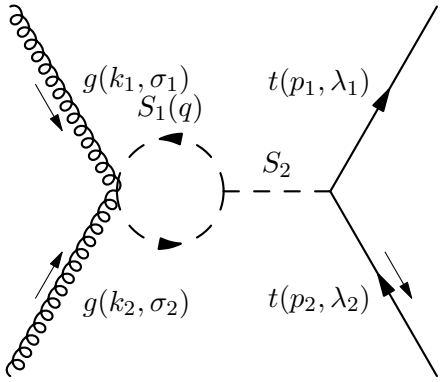

`Dgg_sS_vertSSg`

$S_1 = U_i, D_i \quad , \quad S_2 = H_1^0, A_1^0$

The t-channel vertex corrections are:

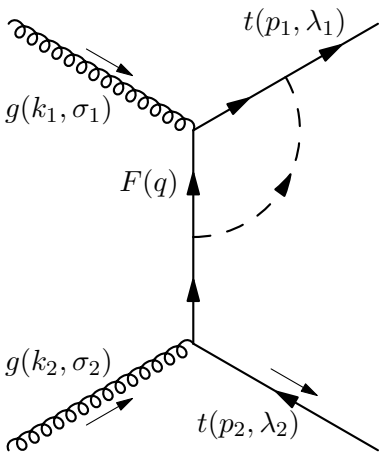

`Dgg_tF_vertS1`*

$(F,S) = (\Lambda, U_i),\ (t, H_1^0),\ (t, A_1^0),\ (b, H_1)$

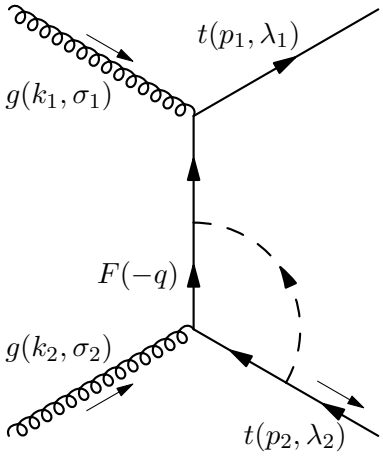

`Dgg_tF_vertS2`*

$(F,S) = (\Lambda, U_i),\ (t, H_1^0),\ (t, A_1^0),\ (b, H_1)$

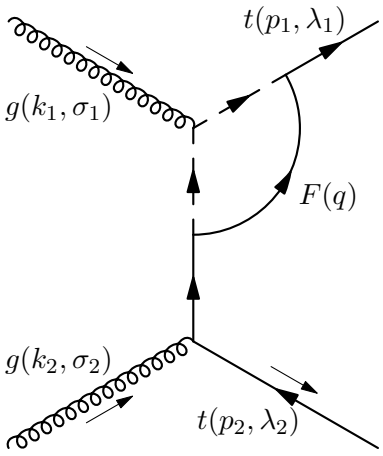

`Dgg_tF_vertSS1`*

$(S,F) = (U_i, \Lambda),\ (U_i, \chi_j^0),\ (D_i, \chi_j)$

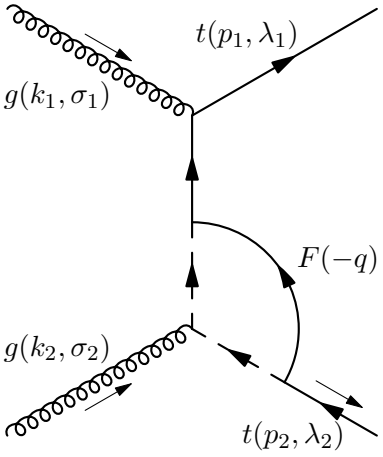

`Dgg_tF_vertSS2`*

$(S,F) = (U_i, \Lambda)$

JHEP11(2007)041

3.4 Box diagrams

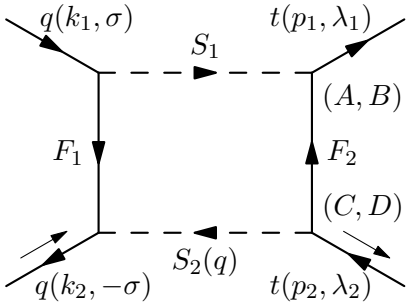

`Dqqbar_boxSS`

$(q, S_1, S_2, F_1, F_2) = (u^I, U_i, U_j, \Lambda, \Lambda),\ (u^I, U_i, U_j, \Lambda, \chi_k^0),\ (u^I, U_i, U_j, \chi_k^0, \Lambda),$
$(d^I, D_i, D_j, \Lambda, \chi_k),\ (d^I, U_i, U_j, \chi_k, \Lambda)$

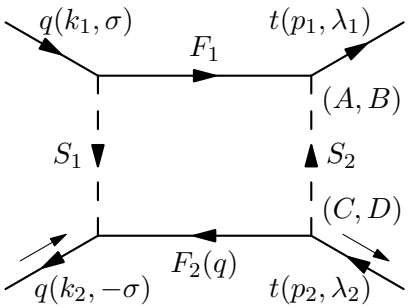

`Dqqbar_fboxSS`

$(q, F_1, F_2, S_1, S_2) = (u^I, \Lambda, \Lambda, U_i, U_j),$
$(d^I, \Lambda, \Lambda, D_i, U_j),\ (u^I, \chi_k^0, \Lambda, U_i, U_j),$
$(u^I, \Lambda, \chi_k^0, U_i, U_j),\ (d^I, \chi_k^0, \Lambda, D_i, U_j),$
$(d^I, \Lambda, \chi_k^0, D_i, U_j)$

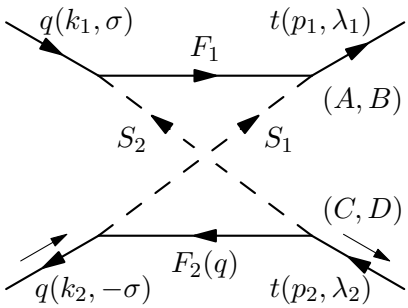

`Dqqbar_fboxSSx`**

$(q, F_1, F_2, S_1, S_2) = (u^I, \Lambda, \Lambda, U_i, U_j),$
$(d^I, \Lambda, \Lambda, D_i, U_j),\ (u^I, \chi_k^0, \Lambda, U_i, U_j),$
$(u^I, \Lambda, \chi_k^0, U_i, U_j),\ (d^I, \chi_k^0, \Lambda, D_i, U_j),$
$(d^I, \Lambda, \chi_k^0, D_i, U_j)$

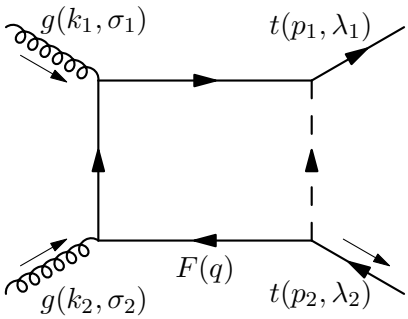

`Dgg_boxFS`*

$(F, S) = (\Lambda, U_i),\ (t, H_1^0),\ (t, A_1^0),\ (b, H_i)$

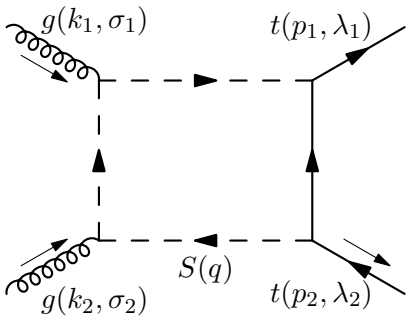

`Dgg_boxSF`*

$(S, F) = (U_i, \Lambda),\ (U_i, \chi_j^0),\ (D_i, \chi_j)$

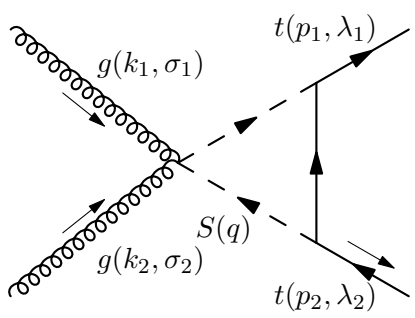

Dgg_boxSF4
$(S, F) = (U_i, \Lambda),\ (U_i, \chi_j^0),\ (D_i, \chi_j)$

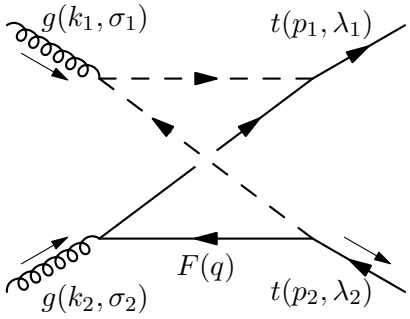

Dgg_boxSFx*
$(S, F) = (U_i, \Lambda)$

4. Cross sections and asymmetries

In this section we present our results for the SUSY corrections to polarised $t\bar{t}$ production cross sections, which we calculated for each of the 10 Snowmass benchmarks detailed in [45]. The benchmarks 1a, 1b and 2 to 6 are derived from gravity mediated SUSY breaking scenarios. Benchmarks 7 and 8 are related to gauge mediated SUSY breaking and benchmark 9 comes from an anomaly mediated scenario. To calculate the masses of the supersymmetric particles and run the couplings to the TeV scale we used the program SOFTSUSY by B. C. Allanach [51]. The renormalisation scale μ of the scale dependent MSSM parameters was set to the geometric mean of the two stop masses, in accordance with the convention adopted in [51]. The decay widths of the MSSM Higgs particles were calculated with the program HDECAY by Djouadi, Kalinowski and Spira [52]. The Feynman rules for the MSSM vertices were taken from J. Rosiek's paper [50]. We compare our parton level cross sections with the results obtained in the leading log approximation [46]. Then we discuss our results for the total $pp \to t\bar{t}$ cross section and double helicity asymmetries.

Let $\hat{\sigma}_i$ denote the total cross section for the process $i \to t\bar{t}$, where the initial state i can be a gluon pair (gg), a light up-type quark-antiquark pair ($u\bar{u}$) or a light down type quark-antiquark pair ($d\bar{d}$). We regard $\hat{\sigma}_i$ as a function of the variable $\hat{s} \equiv M_{t\bar{t}}^2$, where $M_{t\bar{t}}$ is the invariant mass of the top-antitop pair. For each of these cross sections we have calculated the leading order contribution $\hat{\sigma}_i^{\mathrm{LO}}$ and the SUSY corrections $\hat{\sigma}_i^{\mathrm{SUSY}}$ due to the diagrams listed in section 3. The SUSY corrections can be split into super-QCD (SQCD) corrections and super-electroweak (SEW) corrections. The SQCD corrections are of order $\mathcal{O}(\alpha_s^3)$ and the SEW correction of order $\mathcal{O}(\alpha\alpha_s^2)$. Consequently the SEW corrections are one order of magnitude smaller than the SQCD corrections. We also define the ratios

$$\hat{r}_i(\hat{s}) = \frac{\hat{\sigma}_i^{\mathrm{SUSY}}(\hat{s})}{\hat{\sigma}_i^{\mathrm{LO}}(\hat{s})} \quad . \tag{4.1}$$

Figures 5, 6 and 7 show a comparison of the full NLO ratios with the results obtained in the leading log approximation by Beccaria, Renard and Verzegnassi [46]. We have used Snowmass benchmark 5 to compute the cross section, but the observations stated here are true for any of the 10 Snowmass benchmarks. The only SUSY inputs in the leading log approximation are $\tan\beta$ and a universal SUSY mass scale M_{SUSY}. Sensible

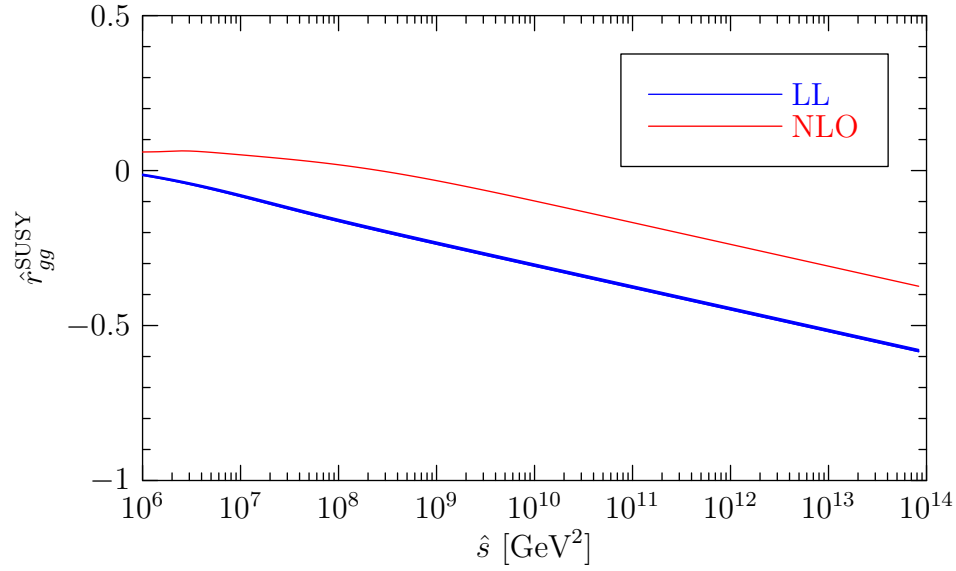

Figure 5: SUSY corrections to the $gg \to t\bar{t}$ cross section in the full NLO calculation and the leading log approximation for benchmark 5 of [45]. The thickness of the leading log graph reflects the uncertainty due to the choice of the universal SUSY scale.

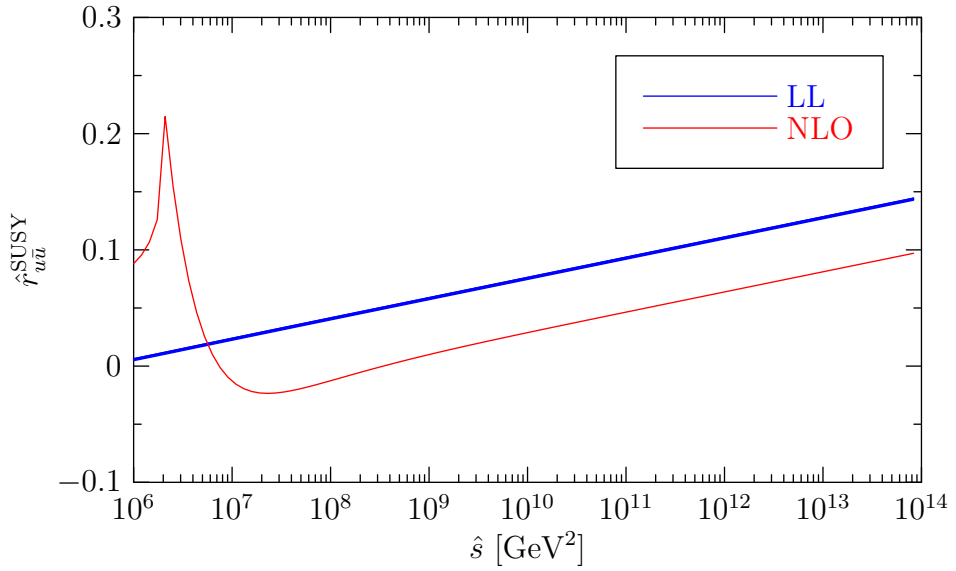

Figure 6: SUSY corrections to the $u\bar{u} \to t\bar{t}$ cross section in full NLO calculation and the leading log approximation for benchmark 5 of [45]. The results for first and second generation up-type quarks are identical. The width of the leading log graph reflects the uncertainty due to the choice of the universal SUSY scale.

values for this scale lie anywhere between the mass of the lightest and the mass of the heaviest SUSY particle. The thickness of the leading log graphs in figures 5, 6 and 7 reflect this uncertainty. We see that, in the leading log approximation, the ratios $\hat{r}_i^{\mathrm{SUSY}}$ are proportional to $\log(\hat{s}/M^2_{\mathrm{SUSY}})$. For $\hat{s} \gtrsim 10^9\,\mathrm{GeV}$ the NLO ratio runs linear with the

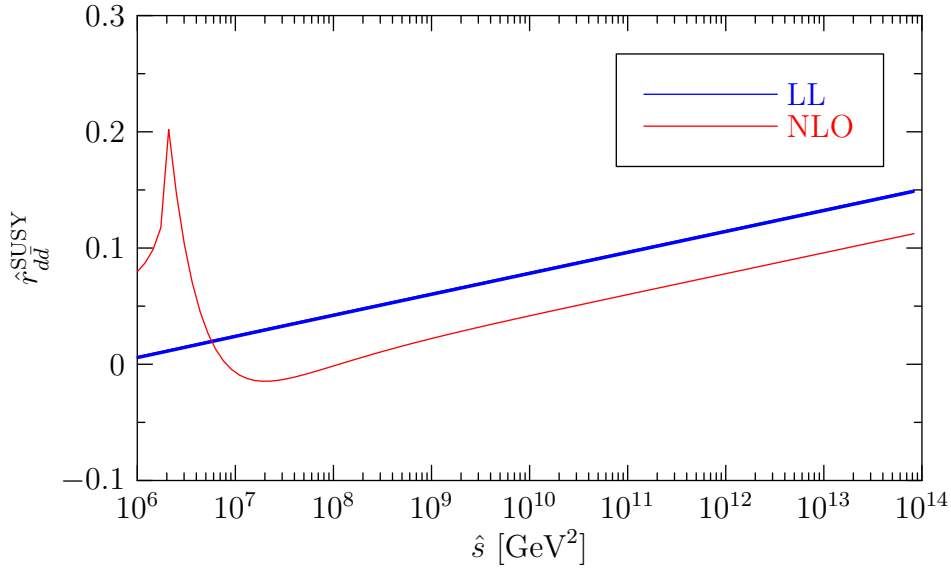

Figure 7: SUSY corrections to the $d\bar{d} \to t\bar{t}$ cross section in the full NLO calculation and the leading log approximation for benchmark 5 of [45]. The results for first and second generation down-type quarks are identical. The width of the leading log graph reflects the uncertainty due to the choice of the universal SUSY scale.

same slope, but with a constant offset to the leading log graph. For very large centre of mass energies this offset becomes small compared with the logrithmic contribution. Therefore our results agree with the leading log approximation in the high energy limit. However, since we can see that the approximation to the corrections consisting of the leading logarithm accompanied by the constant offset is only valid for square energies in excess of approximately $10^8\,\mathrm{GeV}$, it fails totally at energies accessible at LHC for which the entire one-loop correction is needed.

To examine the dependence of these results on $\tan\beta$ we have calculated the ratios $\hat{r}_i$ ($i = gg, u\bar{u}, d\bar{d}$) for different values of $\tan\beta$ in the region where the graphs in figures 5, 6 and 7 run parallel with a constant offset. Figures 8 shows the $\tan\beta$ dependence of the ratios $\hat{r}_i$ at $\hat{s} = 10^{14}\,\mathrm{GeV}^2$. We see that there is only a weak dependence for $\tan\beta < 2$ and a neglegible dependence for $\tan\beta > 2$. In this region the offsets $\Delta\hat{r}_i^{\mathrm{SUSY}}$ between the full NLO and the leading log graphs, which are shown in figure 9, depend on $\tan\beta$, too.

To obtain the $pp \to t\bar{t}$ cross sections, the parton level cross sections $\hat{\sigma}_i$ were folded with the CTEQ6L1 set of the CTEQ v6.51 parton distribution functions [53]. The factorisation scale was set equal to the renormalisation scale. For the proton-proton collision we assumed a centre of mass energy of 14 TeV. Let $d\sigma_{\lambda_1\lambda_2}/dM_{t\bar{t}}$ denote the invariant mass differential cross section for producing a top quark with helicity λ_1 and an anti-top quark with helicity λ_2. Then we define

$$\frac{d\sigma_{\mathrm{tot}}}{dM_{t\bar{t}}} = \frac{d\sigma_{++}}{dM_{t\bar{t}}} + \frac{d\sigma_{--}}{dM_{t\bar{t}}} + \frac{d\sigma_{+-}}{dM_{t\bar{t}}} + \frac{d\sigma_{-+}}{dM_{t\bar{t}}} \quad , \tag{4.2a}$$

$$\frac{d\sigma_{LL}}{dM_{t\bar{t}}} = \frac{d\sigma_{++}}{dM_{t\bar{t}}} + \frac{d\sigma_{--}}{dM_{t\bar{t}}} - \frac{d\sigma_{+-}}{dM_{t\bar{t}}} - \frac{d\sigma_{-+}}{dM_{t\bar{t}}} \quad , \tag{4.2b}$$

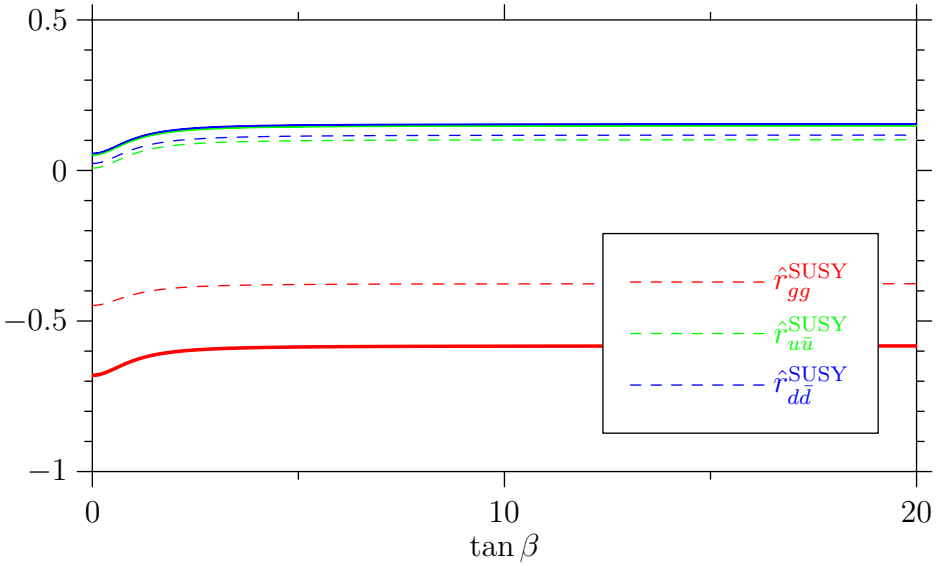

Figure 8: The $\tan\beta$ dependence of the ratios $\hat{r}_{gg}$, $\hat{r}_{u\bar{u}}$ and $\hat{r}_{d\bar{d}}$ at $\hat{s} = 10^{14}\,\mathrm{GeV}^2$. The solid lines are the results in the leading log approximation. Their thickness reflects the uncertainty with due to the choice of the universal SUSY scale. The dashed lines are the results of the full NLO calculation.

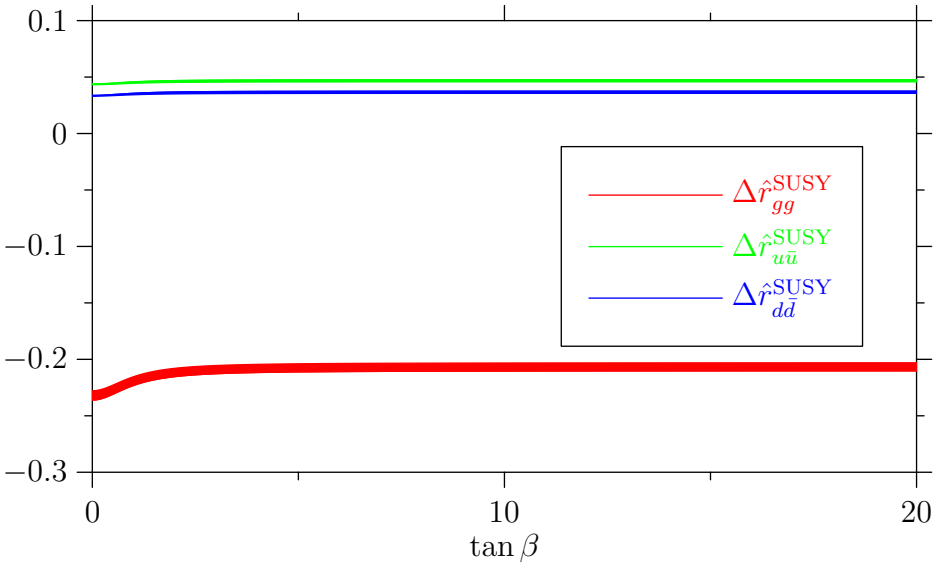

Figure 9: The $\tan\beta$ dependence of the offsets $\Delta\hat{r}_{gg}$, $\Delta\hat{r}_{u\bar{u}}$ and $\Delta\hat{r}_{d\bar{d}}$ at $\hat{s} = 10^{14}\,\mathrm{GeV}^2$. These are the differences between the solid and the dashed lines in figure 8. The thickness of the lines reflects the uncertainty with due to the choice of the universal SUSY scale.

$$\frac{d\sigma_{PV}}{dM_{t\bar{t}}} = \frac{d\sigma_{+-}}{dM_{t\bar{t}}} - \frac{d\sigma_{-+}}{dM_{t\bar{t}}} \quad . \tag{4.2c}$$

For each combination we indicate the leading order and SUSY contributions by superscripts 'LO' and 'SUSY', respectively. The parity even combinations $d\sigma_{\rm tot}^{\rm SUSY}$ and $d\sigma_{LL}^{\rm SUSY}$ are dominated by the SQCD corrections. However, for the parity odd combination $d\sigma_{PV}^{\rm SUSY}$ the

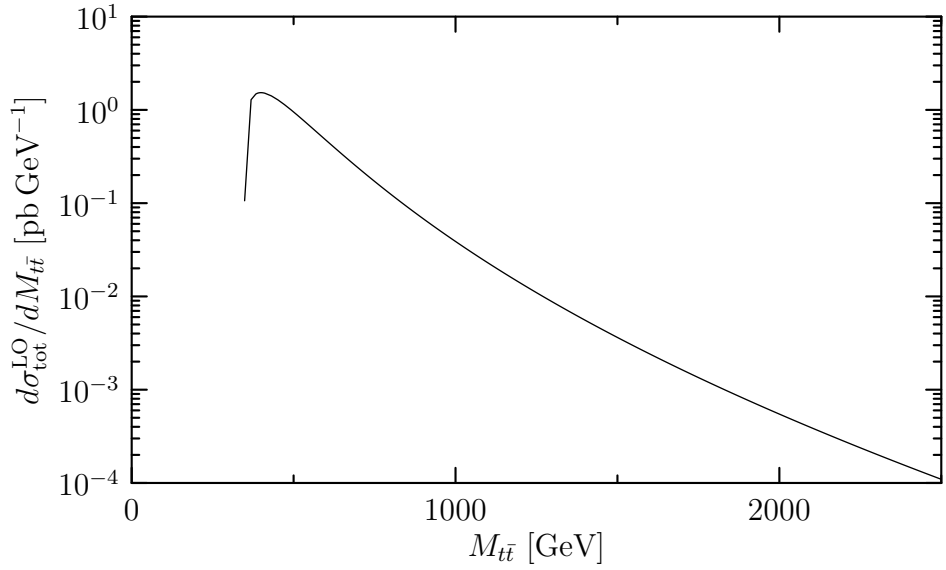

Figure 10: Leading order results for the invariant mass differential cross section. The renormalisation and factorisation scales are set to 464 GeV.

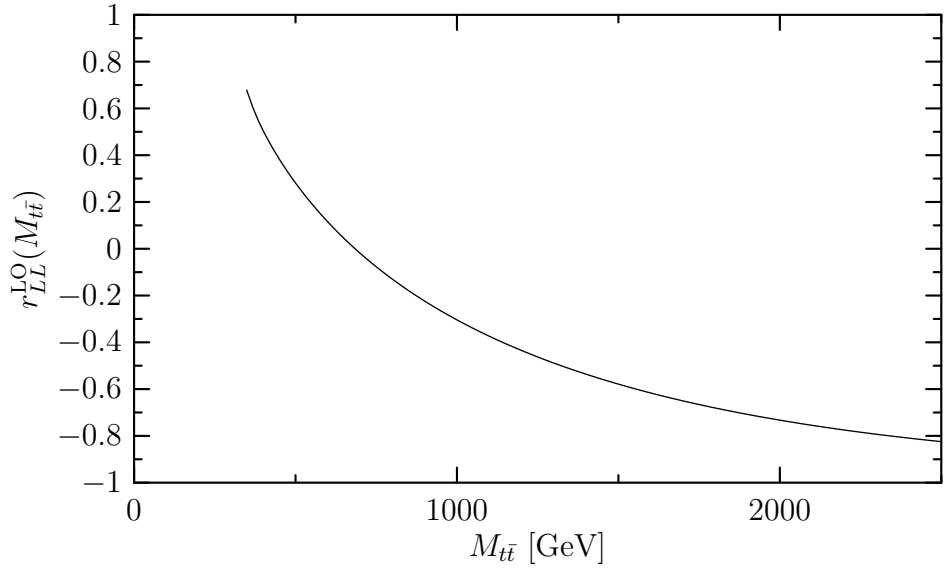

Figure 11: Leading order results for the invariant mass LL asymmetry. The renormalisation and factorisation scales are set to 464 GeV.

SQCD corrections are zero, since parity is conserved in super-QCD. For the asymmetries and the SUSY corrections we define the ratios

$$r^{\rm LO}_{LL/PV}(M_{t\bar{t}}) = \frac{d\sigma^{\rm LO}_{LL/PV}/dM_{t\bar{t}}}{d\sigma^{\rm LO}_{\rm tot}/dM_{t\bar{t}}} \quad , \quad r^{\rm SUSY}_{{\rm tot}/LL/PV}(M_{t\bar{t}}) = \frac{d\sigma^{\rm SUSY}_{{\rm tot}/LL/PV}/dM_{t\bar{t}}}{d\sigma^{\rm LO}_{\rm tot}/dM_{t\bar{t}}} \quad . \quad (4.3)$$

Figures 10 and 11 show the results for $d\sigma^{\rm LO}_{\rm tot}/dM_{t\bar{t}}$ and $r^{\rm LO}_{LL}(M_{t\bar{t}})$, respectively, with a renormalisation scale $\mu = 464\,\text{GeV}$ (corresponding to the geometric mean of the stop

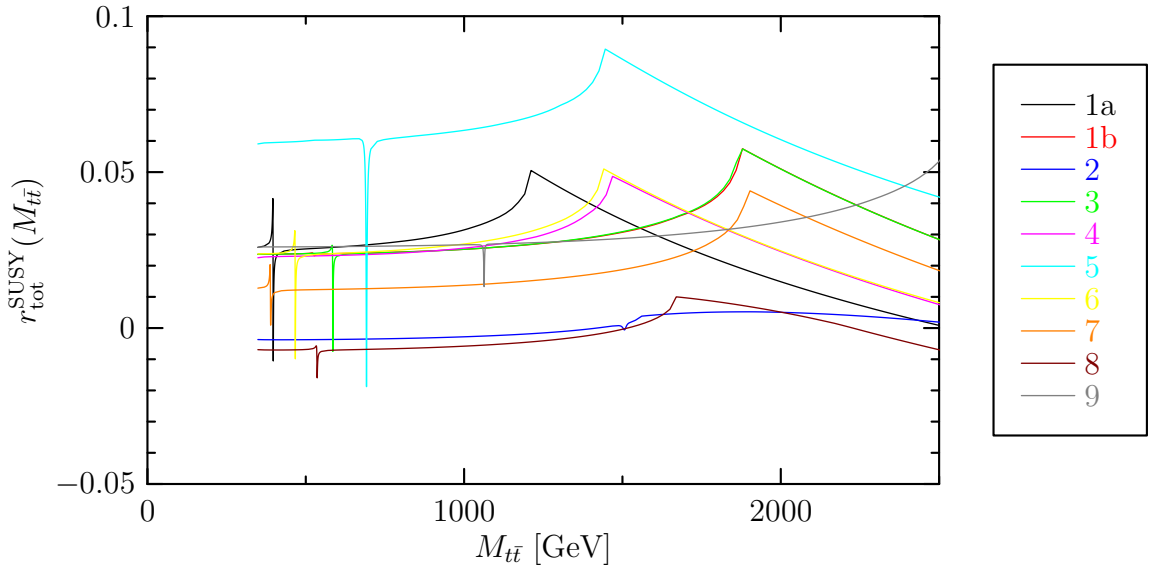

Figure 12: SUSY corrections to the invariant mass differential cross section for the Snowmass benchmarks. The numbers in the legend refer to the labelling of the benchmarks in [45].

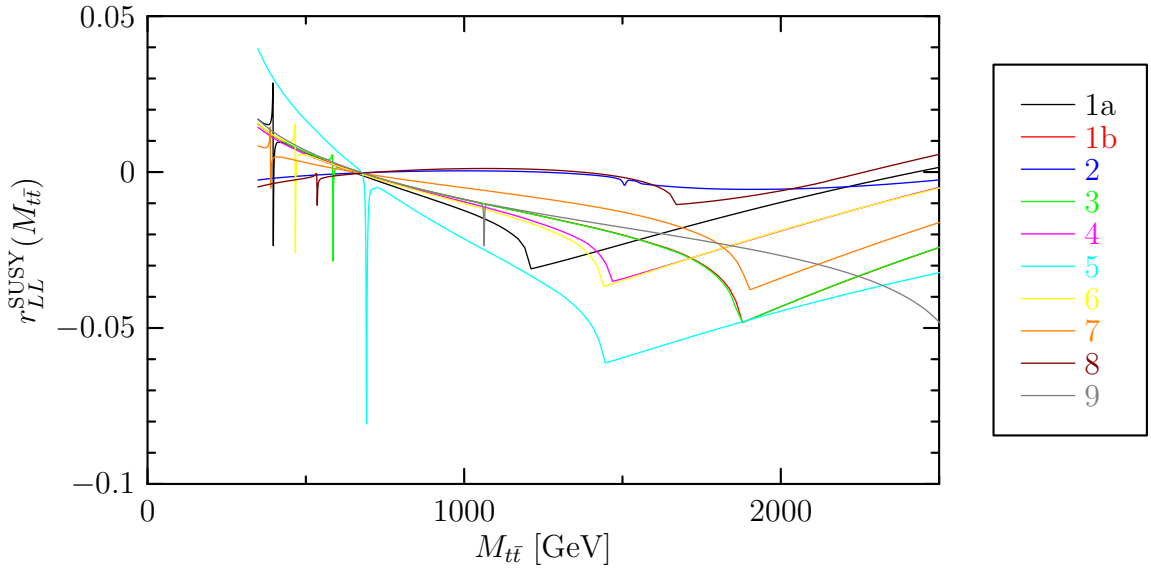

Figure 13: SUSY corrections to the invariant mass LL asymmetry for the Snowmass benchmarks. The numbers in the legend refer to the labelling of the benchmarks in [45].

masses in benchmark 1a). Since there is no parity violation at leading order the ratio $r_{PV}^{\rm LO}$ is identically zero.

Figures 12 and 13 show the ratios $r_{\rm tot}^{\rm SUSY}(M_{t\bar{t}})$ and $r_{LL}^{\rm SUSY}(M_{t\bar{t}})$ for each of the 10 Snowmass benchmarks. The renormalisation and factorisation scales are set, for each benchmark, to the geometric mean of the stop masses. The numerical values are shown

JHEP11(2007)041

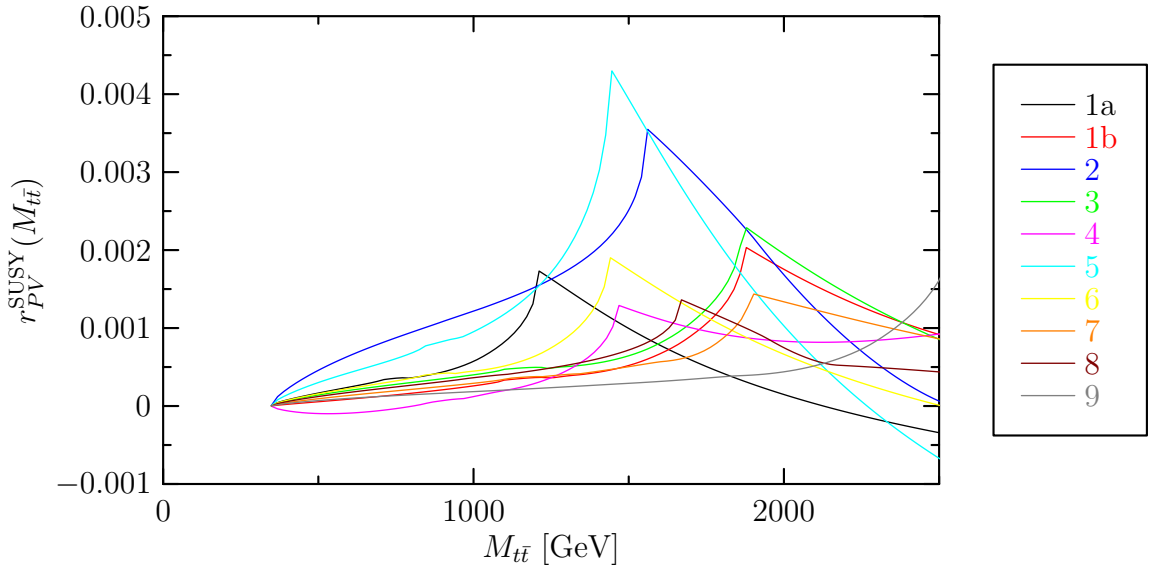

Figure 14: SUSY corrections to the invariant mass PV asymmetry for the Snowmass benchmarks. The numbers in the legend refer to the labelling of the benchmarks in [45].

in table 1. We have added up the super-electroweak (SEW) and super-QCD (SQCD) corrections, but the SEW corrections are negligible compared to the SQCD corrections. We see that the SUSY corrections to the $t\bar{t}$ cross section can be as large as 10% of the leading order cross section, but typically only reach the 5% level. In both plots we see "resonance peaks" located at the masses of the heavy and the pseudo-scalar Higgs (H_1^0 and A_1^0 in the notation of [50]). They come from the scalar s-channel propagators in the diagrams labelled `Dgg_sS_vertFg`, `Dgg_sS_vertSg` and `Dgg_sS_vertSSg` in section 3. Note that due to the fermion triangle the sign of the diagram `Dgg_sS_vertFg` is opposite that of `Dgg_sS_vertSg` and `Dgg_sS_vertSSg`. This explains why we get "troughs" instead of peaks for some of the benchmarks. Also note that, for all 10 benchmarks, the difference of the heavy and the pseudo-scalar Higgs masses is much smaller than their decay widths. Consequently we can only see two distinct peaks when these peaks have opposite signs. The kinks occurring between 1 and 2 TeV coincide, for each benchmark, with twice the gluino mass and can therefore be understood as a threshold effect due to the box diagrams `Dqqbar_fboxSS` and `Dgg_boxFS`.

Figure 14 shows the SUSY corrections to the parity violating asymmetry for each of the 10 benchmarks. Here the resonance peaks are absent, because the diagrams `Dgg_sS_vertFg`, `Dgg_sS_vertSg` and `Dgg_sS_vertSSg` are parity-conserving. Furthermore, the SUSY corrections to the parity violating asymmetry are one order of magnitude smaller than the corrections to the parity-even observables, because it only gets super-electroweak contributions of order $\mathcal{O}(\alpha\alpha_s^2)$.

By integrating the differential cross sections (4.2) over $M_{t\bar{t}}$ we obtain cross sections for producing $t\bar{t}$ pairs with arbitrary invariant mass. We define the cross sections σ_{tot}, σ_{LL}

	μ	$\sigma_{\rm tot}^{\rm LO}$	$\sigma_{\rm tot}^{\rm SUSY}$	$\sigma_{LL}^{\rm LO}$	$\sigma_{LL}^{\rm SUSY}$	$\sigma_{PV}^{\rm SUSY}$
1a	465	331.8	+8.5	91.99	+1.83	+0.063
1b	719	288.3	+6.9	79.50	+1.74	+0.020
2	1100	266.3	−1.0	72.84	−0.33	+0.125
3	713	289.5	+6.9	80.08	+1.75	+0.043
4	595	307.6	+7.2	85.62	+1.68	−0.018
5	402	332.1	+19.9	93.48	+5.19	+0.111
6	559	310.8	+7.4	85.74	+1.73	+0.053
7	820	284.9	+3.5	78.04	+0.80	+0.029
8	1013	271.2	−1.9	74.08	−0.62	+0.035
9	992	263.6	+6.9	72.32	+1.83	+0.019

Table 1: Numerical results for the integrated $t\bar{t}$ cross section and asymmetries. The numbers in the left column refer to the labelling of the Snowmass benchmarks in [45]. The renormalisation scale μ in the second column is given in GeV. The superscripts 'LO' and 'SUSY' indicate leading order results and SUSY corrections, respectively. The cross sections are given in pico-barns (pb).

and σ_{PV} by

$$\sigma_{\rm tot/LL/PV} = \int_{2m_t}^{M_{pp}} dM_{t\bar{t}} \frac{d\sigma_{\rm tot/LL/PV}}{dM_{t\bar{t}}} \quad , \tag{4.4}$$

where m_t is the top mass and $M_{pp} = 14\,\text{TeV}$ is the invariant mass of the proton-proton system. Again, the leading order and SUSY contributions are indicated by superscripts 'LO' and 'SUSY', respectively. Table 1 summarises our results for these cross sections. For both, $\sigma_{\rm tot}$ and σ_{LL} we see that the SUSY corrections typically make up 2% of the leading order results. However, they can be as big as 5% in the case of benchmark 5 and as small as 0.3% in the case of benchmark 2.

Experimentally it is often more convenient to parametrise the $t\bar{t}$ production cross section by the transverse momentum p_T of the top quark. For the transverse momentum differential cross section $d\sigma_{\lambda_1\lambda_2}/dp_T$ we define the total differential cross section $d\sigma_{\rm tot}/dp_T$, the asymmetries $d\sigma_{LL}/dp_T$ and $d\sigma_{PV}/dp_T$ and the ratios $r_{LL}^{\rm LO}(p_T)$, $r_{PV}^{\rm LO}(p_T)$, $r_{\rm tot}^{\rm SUSY}(p_T)$, $r_{LL}^{\rm SUSY}(p_T)$ and $r_{PV}^{\rm SUSY}(p_T)$ in analogy to (4.2) and (4.3). Our results for these quantities are shown in figures 15 to 19. We note here that the "resonance peaks" and "troughs" from the thresholds for scalar particle exchange are smoothed out by the phase-space integration which means that $M_{t\bar{t}}$ is a far better variable in which to analyse the data in order to extract information on the SUSY parameter set, although we note that some of the benchmarks give rise to an enhancement of the differential cross-section of up to 7% at large p_T.

5. Conclusions

We have calculated the complete MSSM corrections to the cross-section for $t\bar{t}$ production at the LHC. The calculation has been set up in terms of prototype Feynman graphs for the polarised amplitudes at parton-level. These prototypes are independent of the underlying model and can be re-used for studying the effects of other BSM physics on top-quark

JHEP11(2007)041

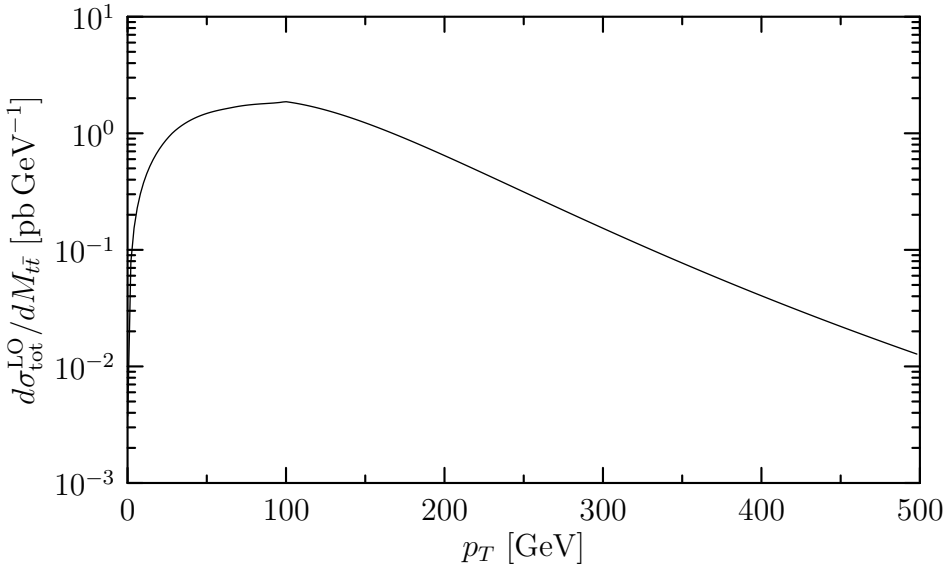

Figure 15: Leading order results for the transverse momentum differential cross section.

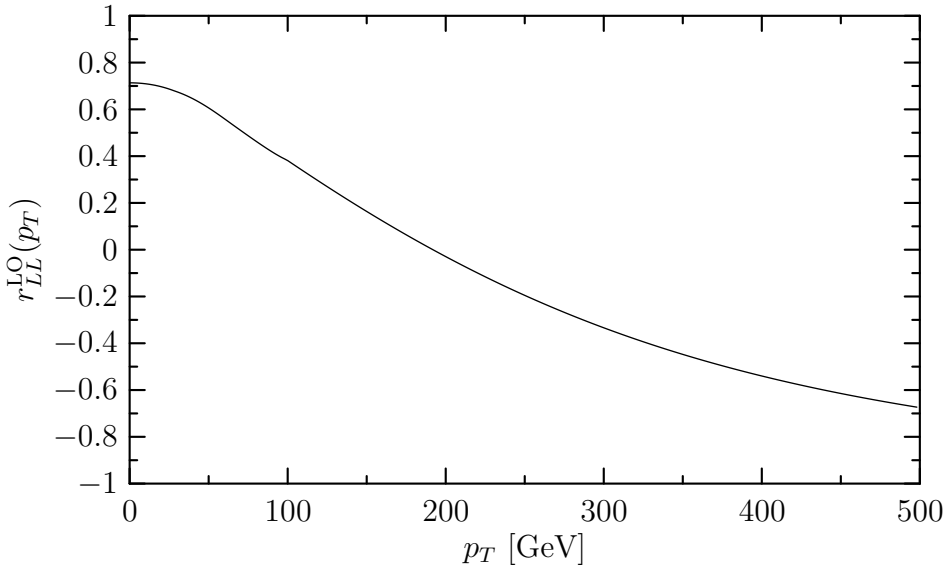

Figure 16: Leading order results for the transverse momentum LL asymmetry.

production. In a second step we used these prototypes to construct a numerical library that computes the MSSM corrections for arbitrary values of the full set of MSSM parameters.

As a first analysis we have calculated numerical results for the ten Snowmass benchmark sets using the CTEQ PDFs. We find a considerable variation of the effects of the one-loop SUSY corrections between the various benchmarks. The benchmark giving the largest correction is benchmark 5, which is a super-gravity model with small $\tan\beta = 5$ and a large negative tri-linear coupling, $A_0 = -1000\,\text{GeV}$. These large corrections can be understood from the fact that this large tri-linear coupling generates a light stop mass

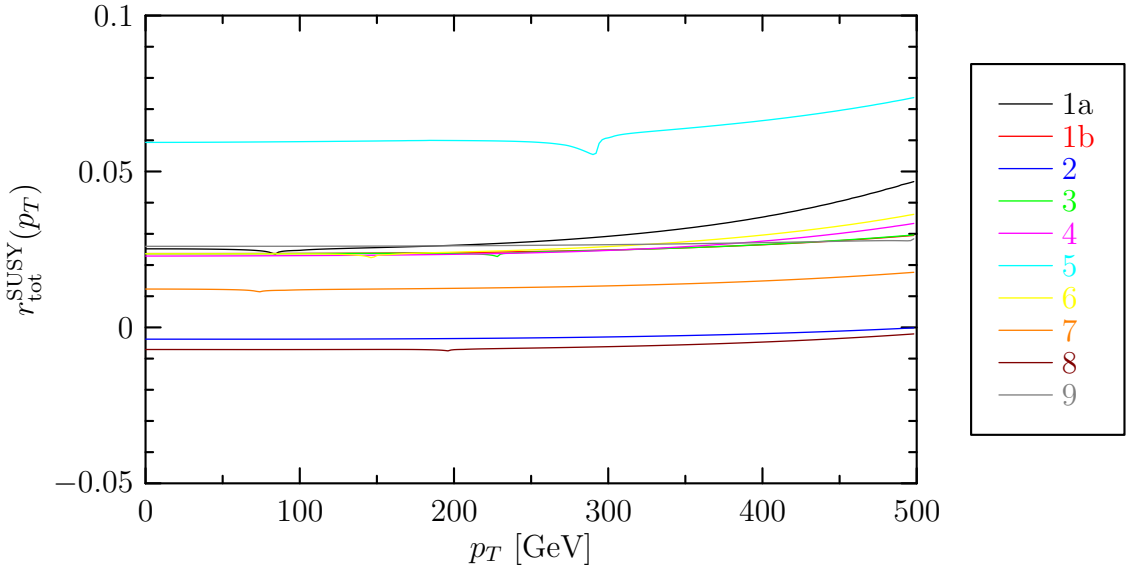

Figure 17: SUSY corrections to the transverse momentum differential cross section for the Snowmass benchmarks. The numbers in the legend refer to the labelling of the benchmarks in [45].

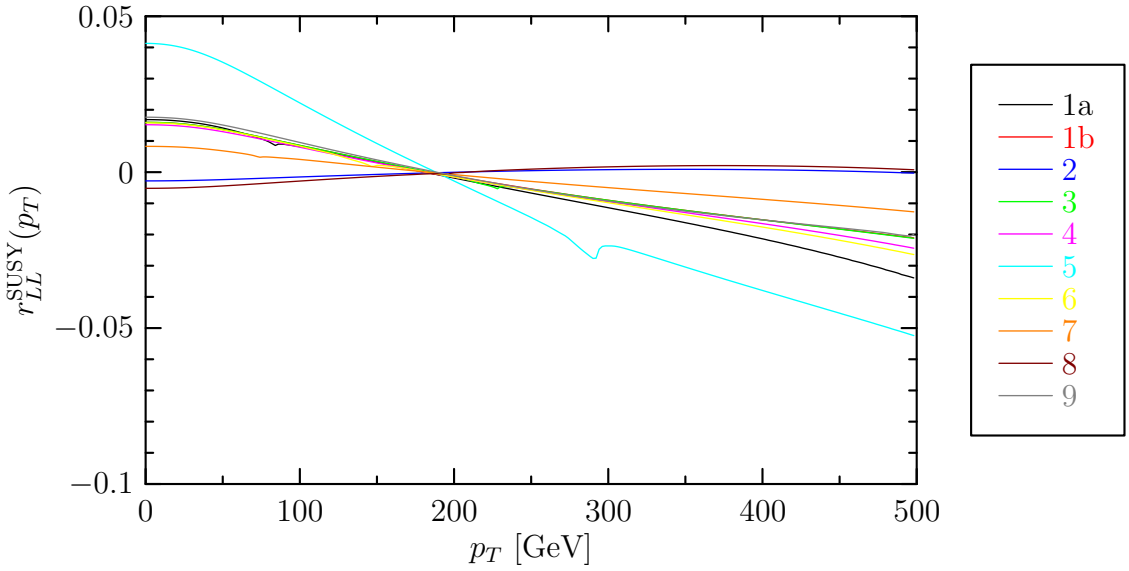

Figure 18: SUSY corrections to the transverse momentum LL asymmetry for the Snowmass benchmarks. The numbers in the legend refer to the labelling of the benchmarks in [45].

(258 GeV) thereby enhancing graphs involving a stop mass inside the loop. This gives an enhancement of 6% in the total production cross-section.

Whereas the corrections for the other benchmarks are somewhat smaller, they are usually around 3% and therefore comparable to the weak corrections calculated by Bernreuther et. al. [31] and Kühn et. al. [20]. Note that whereas the weak corrections reported in [31, 20] *decrease* the prediction for the cross-sections, the SUSY corrections have a *positive* sign for most of the benchmarks considered.

JHEP11(2007)041

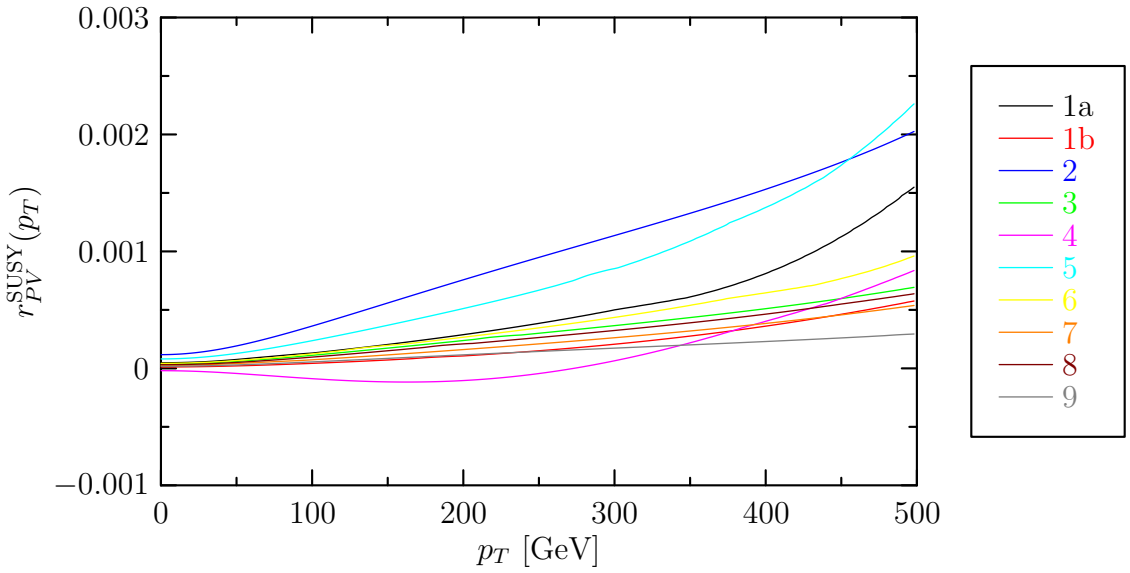

Figure 19: SUSY corrections to the transverse momentum PV asymmetry for the Snowmass benchmarks. The numbers in the legend refer to the labelling of the benchmarks in [45].

Statistically, we expect these events to be easily detectable given the anticipated yield of order 10^7 events over the period of running of the LHC. We have found similar corrections in the asymmetry ratios defined in in (4.2) and (4.3). For these asymmetries we also expect cancellation of systematic errors arising from uncertainties in incoming parton fluxes and tagging efficiencies, so that these corrections of order 3% would exceed the statistical errors by a factor of ~ 100.

Given corrections of such significance, it is reasonable to assume that corrections in the differential cross-sections will also be detectable (provided sufficiently large bins are taken). We have therefore plotted the differential cross-sections with respect to the invariant mass $M_{t\bar{t}}$ of the $t\bar{t}$ system and also with respect to the transverse momentum p_T of the t-quark. In the former case, the differential cross-sections display an interesting structure with peaks and/or troughs corresponding to thresholds for scalar particle exchanges in the gluon fusion process.

We have also determined the SUSY contribution to the parity odd helicity asymmetry. This receives only contributions from the supersymmetric partners in the weak-interaction sector, which are suppressed relative to the SQCD corrections by $\mathcal{O}(\alpha_W/\alpha_s)$. It would appear, therefore that even for benchmark 5, which produces the largest corrections, such parity violating asymmetries will be too small to observe.

Acknowledgments

The authors are grateful to Stefano Moretti and Sacha Belyaev for useful converstaions.

References

[1] J. Wess and B. Zumino, *Supergauge transformations in four-dimensions*, *Nucl. Phys.* **B 70** (1974) 39.

[2] S. Dimopoulos and H. Georgi, *Softly broken supersymmetry and* SU(5), *Nucl. Phys.* **B 193** (1981) 150.

[3] J.H. Kühn, *How to measure the polarization of top quarks*, *Nucl. Phys.* **B 237** (1984) 77.

[4] A. Brandenburg, *Spin-spin correlations of top quark pairs at hadron colliders*, *Phys. Lett.* **B 388** (1996) 626 [hep-ph/9603333].

[5] H.M. Georgi, S.L. Glashow, M.E. Machacek and D.V. Nanopoulos, *Charmed particles from two - gluon annihilation in proton proton collisions*, *Ann. Phys. (NY)* **114** (1978) 273.

[6] B.L. Combridge, *Associated production of heavy flavor states in p p and $\bar{p}p$ interactions: some QCD estimates*, *Nucl. Phys.* **B 151** (1979) 429.

[7] M. Glück, J.F. Owens and E. Reya, *Gluon contribution to hadronic j/ψ production*, *Phys. Rev.* **D 17** (1978) 2324.

[8] J. Babcock, D.W. Sivers and S. Wolfram, *QCD estimates for heavy particle production*, *Phys. Rev.* **D 18** (1978) 162.

[9] K. Hagiwara and T. Yoshino, *Hadroproduction of heavy quark flavors in QCD*, *Phys. Lett.* **B 80** (1979) 282.

[10] L.M. Jones and H.W. Wyld, *On hadronic charm production by gluon fusion*, *Phys. Rev.* **D 17** (1978) 1782.

[11] P. Nason, S. Dawson and R.K. Ellis, *The total cross-section for the production of heavy quarks in hadronic collisions*, *Nucl. Phys.* **B 303** (1988) 607.

[12] W. Beenakker, H. Kuijf, W.L. van Neerven and J. Smith, *QCD corrections to heavy quark production in $p\bar{p}$ collisions*, *Phys. Rev.* **D 40** (1989) 54.

[13] G. Altarelli, M. Diemoz, G. Martinelli and P. Nason, *Total cross-sections for heavy flavor production in hadronic collisions and QCD*, *Nucl. Phys.* **B 308** (1988) 724.

[14] W. Beenakker, W.L. van Neerven, R. Meng, G.A. Schuler and J. Smith, *QCD corrections to heavy quark production in hadron hadron collisions*, *Nucl. Phys.* **B 351** (1991) 507.

[15] M.L. Mangano, P. Nason and G. Ridolfi, *Heavy quark correlations in hadron collisions at next-to-leading order*, *Nucl. Phys.* **B 373** (1992) 295.

[16] S. Frixione, M.L. Mangano, P. Nason and G. Ridolfi, *Top quark distributions in hadronic collisions*, *Phys. Lett.* **B 351** (1995) 555 [hep-ph/9503213].

[17] W. Beenakker et al., *Electroweak one loop contributions to top pair production in hadron colliders*, *Nucl. Phys.* **B 411** (1994) 343.

[18] J.H. Kühn, A. Scharf and P. Uwer, *Electroweak corrections to top-quark pair production in quark-antiquark annihilation*, *Eur. Phys. J.* **C 45** (2006) 139 [hep-ph/0508092].

[19] S. Moretti, M.R. Nolten and D.A. Ross, *Weak corrections to four-parton processes*, *Nucl. Phys.* **B 759** (2006) 50 [hep-ph/0606201].

[20] J.H. Kühn, A. Scharf and P. Uwer, *Electroweak effects in top-quark pair production at hadron colliders*, *Eur. Phys. J.* **C 51** (2007) 37 [hep-ph/0610335].

JHEP11(2007)041

[21] N. Kidonakis and R. Vogt, *Next-to-next-to-leading order soft-gluon corrections in top quark hadroproduction*, *Phys. Rev.* **D 68** (2003) 114014 [hep-ph/0308222].

[22] R. Bonciani, S. Catani, M.L. Mangano and P. Nason, *NLL resummation of the heavy-quark hadroproduction cross-section*, *Nucl. Phys.* **B 529** (1998) 424 [hep-ph/9801375].

[23] N. Kidonakis, E. Laenen, S. Moch and R. Vogt, *Sudakov resummation and finite order expansions of heavy quark hadroproduction cross sections*, *Phys. Rev.* **D 64** (2001) 114001 [hep-ph/0105041].

[24] N. Kidonakis and R. Vogt, *Theoretical status of the top quark cross section*, *Int. J. Mod. Phys.* **A 20** (2005) 3171 [hep-ph/0410367].

[25] A. Banfi and E. Laenen, *Joint resummation for heavy quark production*, *Phys. Rev.* **D 71** (2005) 034003 [hep-ph/0411241].

[26] W. Bernreuther, A. Brandenburg and Z.G. Si, *Next-to-leading order QCD corrections to top quark spin correlations at hadron colliders: the reactions $q\bar{q} \to t\bar{t}(g)$*, *Phys. Lett.* **B 483** (2000) 99 [hep-ph/0004184].

[27] W. Bernreuther, A. Brandenburg, Z.G. Si and P. Uwer, *Top quark spin correlations at hadron colliders: predictions at next-to-leading order QCD*, *Phys. Rev. Lett.* **87** (2001) 242002 [hep-ph/0107086].

[28] W. Bernreuther, A. Brandenburg, Z.G. Si and P. Uwer, *Next-to-leading order QCD corrections to top quark spin correlations at hadron colliders: the reactions $gg \to t\bar{t}(g)$ and $gq(\bar{q}) \to t\bar{t}q(\bar{q})$*, *Phys. Lett.* **B 509** (2001) 53 [hep-ph/0104096].

[29] W. Bernreuther, A. Brandenburg, Z.G. Si and P. Uwer, *Top quark pair production and decay at hadron colliders*, *Nucl. Phys.* **B 690** (2004) 81 [hep-ph/0403035].

[30] C. Kao and D. Wackeroth, *Parity violating asymmetries in top pair production at hadron colliders*, *Phys. Rev.* **D 61** (2000) 055009 [hep-ph/9902202].

[31] W. Bernreuther, M. Fücker and Z.-G. Si, *Weak interaction corrections to hadronic top quark pair production*, *Phys. Rev.* **D 74** (2006) 113005 [hep-ph/0610334].

[32] C. Kao, G.A. Ladinsky and C.P. Yuan, *Leading weak corrections to the production of heavy top quarks at hadron colliders*, *Int. J. Mod. Phys.* **A 12** (1997) 1341.

[33] W. Bernreuther, M. Fuecker and Z.G. Si, *Mixed QCD and weak corrections to top quark pair production at hadron colliders*, *Phys. Lett.* **B 633** (2006) 54 [hep-ph/0508091].

[34] S. Moretti, M.R. Nolten and D.A. Ross, *Weak corrections to gluon-induced top-antitop hadro-production*, *Phys. Lett.* **B 639** (2006) 513 [hep-ph/0603083].

[35] J.M. Yang and C.S. Li, *Top squark mixing effects in the supersymmetric electroweak corrections to top quark production at the Tevatron*, *Phys. Rev.* **D 54** (1996) 4380 [hep-ph/9603442].

[36] J. Kim, J.L. Lopez, D.V. Nanopoulos and R. Rangarajan, *Enhanced supersymmetric corrections to top-quark production at the Tevatron*, *Phys. Rev.* **D 54** (1996) 4364 [hep-ph/9605419].

[37] W. Hollik, W.M. Mosle and D. Wackeroth, *Top pair production at hadron colliders in non-minimal standard models*, *Nucl. Phys.* **B 516** (1998) 29 [hep-ph/9706218].

JHEP11(2007)041

[38] H.-Y. Zhou and C.-S. Li, *Supersymmetric QCD corrections to top quark pair production at CERN LHC*, *Phys. Rev.* **D 55** (1997) 4421.

[39] Z.-H. Yu, H. Pietschmann, W.-G. Ma, L. Han and J. Yi, *Top-quark pair production via polarized and unpolarized protons in the supersymmetric QCD*, *Eur. Phys. J.* **C 9** (1999) 463 [hep-ph/9804331].

[40] S. Alam, K. Hagiwara, S. Matsumoto, K. Hagiwara and S. Matsumoto, *One loop supersymmetric QCD radiative corrections to the top quark production in $p\bar{p}$ collisions. (revised version)*, *Phys. Rev.* **D 55** (1997) 1307 [hep-ph/9607466].

[41] Z. Sullivan, *Supersymmetric QCD correction to top-quark production at the Tevatron*, *Phys. Rev.* **D 56** (1997) 451 [hep-ph/9611302].

[42] D. Wackeroth, *Loop-induced SUSY effects in strong top pair production*, hep-ph/9807558.

[43] S. Berge, W. Hollik, W.M. Mosle and D. Wackeroth, *SUSY QCD one-loop effects in (un)polarized top-pair production at hadron colliders*, *Phys. Rev.* **D 76** (2007) 034016 [hep-ph/0703016].

[44] P. Skands et al., *SUSY Les Houches accord: interfacing SUSY spectrum calculators, decay packages and event generators*, *JHEP* **07** (2004) 036 [hep-ph/0311123].

[45] B.C. Allanach et al., *The snowmass points and slopes: benchmarks for SUSY searches*, hep-ph/0202233.

[46] M. Beccaria, F.M. Renard and C. Verzegnassi, *Supersymmetric virtual effects in heavy quark pair production at LHC*, *Phys. Rev.* **D 69** (2004) 113004 [hep-ph/0402028].

[47] G. Passarino and M.J.G. Veltman, *One loop corrections for e^+e^- annihilation into $\mu^+\mu^-$ in the Weinberg model*, *Nucl. Phys.* **B 160** (1979) 151.

[48] G.J. van Oldenborgh and J.A.M. Vermaseren, *New algorithms for one loop integrals*, *Z. Physik* **C 46** (1990) 425.

[49] T. Hahn and M. Pérez-Victoria, *Automatized one-loop calculations in four and D dimensions*, *Comput. Phys. Commun.* **118** (1999) 153 [hep-ph/9807565].

[50] J. Rosiek, *Complete set of Feynman rules for the MSSM – erratum*, hep-ph/9511250.

[51] B.C. Allanach, *Softsusy: a C++ program for calculating supersymmetric spectra*, *Comput. Phys. Commun.* **143** (2002) 305 [hep-ph/0104145].

[52] A. Djouadi, J. Kalinowski and M. Spira, *HDECAY: a program for Higgs boson decays in the standard model and its supersymmetric extension*, *Comput. Phys. Commun.* **108** (1998) 56 [hep-ph/9704448].

[53] J. Pumplin et al., *New generation of parton distributions with uncertainties from global QCD analysis*, *JHEP* **07** (2002) 012 [hep-ph/0201195].

JHEP11(2007)041